© 2020. Published by The Company of Biologists Ltd | Journal of Cell Science (2020) 133, jcs232835. doi:10.1242/jcs.232835

RESEARCH ARTICLE

A GTPase-induced switch in phospholipid affinity of collybistin contributes to synaptic gephyrin clustering

Markus Kilisch[1], Simone Mayer[2,*], Miso Mitkovski[3], Heiko Roehse[3], Jennifer Hentrich[1], Blanche Schwappach[1] and Theofilos Papadopoulos[1,‡]

ABSTRACT

Synaptic transmission between neurons relies on the exact spatial organization of postsynaptic transmitter receptors, which are recruited and positioned by dedicated scaffolding and regulatory proteins. At GABAergic synapses, the regulatory protein collybistin (Cb, also known as ARHGEF9) interacts with small GTPases, cell adhesion proteins and phosphoinositides to recruit the scaffolding protein gephyrin and $GABA_A$ receptors to nascent synapses. We dissected the interaction of Cb with the small Rho-like GTPase TC10 (also known as RhoQ) and phospholipids. Our data define a protein–lipid interaction network that controls the clustering of gephyrin at synapses. Within this network, TC10 and monophosphorylated phosphoinositides, particulary phosphatidylinositol 3-phosphate (PI3P), provide a coincidence detection platform that allows the accumulation and activation of Cb in endomembranes. Upon activation, TC10 induces a phospholipid affinity switch in Cb, which allows Cb to specifically interact with phosphoinositide species present at the plasma membrane. We propose that this GTPase-based regulatory switch mechanism represents an important step in the process of tethering of Cb-dependent scaffolds and receptors at nascent postsynapses.

KEY WORDS: $GABA_A$ receptors, Synaptogenesis, Inhibition, Postsynaptic scaffold

INTRODUCTION

Fast chemical synaptic transmission between neurons requires the tight clustering of ionotropic neurotransmitter receptors in the postsynaptic plasma membrane. Apart from the cognate $GABA_A$ receptors ($GABA_A$Rs) (Luscher et al., 2011), core components of many inhibitory GABAergic postsynapses are the cell adhesion proteins neuroligin 2 (NL2, also known as NLGN2) and neuroligin 4 (NL4, also known as NLGN4) (Hoon et al., 2011; Poulopoulos et al., 2009), the scaffolding protein gephyrin (Feng et al., 1998), and the guanine nucleotide exchange factor (GEF) collybistin (Cb, also known as ARHGEF9) (Kins et al., 2000), which together control $GABA_A$R recruitment to synapses. Correspondingly, loss of Cb leads to a massive reduction of gephyrin and $GABA_A$R clusters in several regions of the forebrain (Papadopoulos et al., 2008, 2007). This indicates that Cb there has an essential role in the initial assembly and maintenance of GABAergic postsynapses.

All known mRNAs generated from the single Cb gene in rodents encode tandem Dbl-homology (DH) and pleckstrin-homology (PH) domains, and the vast majority encode an additional N-terminal Src-homology 3 (SH3) domain (Harvey et al., 2004). Furthermore, rodents express three Cb splice variants (CbI, CbII and CbIII) that differ in their C-terminus (Harvey et al., 2004). Of these, only CbII and CbIII are expressed in adult neurons (Harvey et al., 2004). A previous report indicates that CbI and CbII differentially regulate GABAergic synapse formation during development, and that the functional specialization of these Cb isoforms arises from their differential protein half-life, which is controlled through ubiquitin conjugation at the unique CbI C-terminus (de Groot et al., 2017). Instead, CbII and CbIII do not differ with regard to postsynaptic targeting and their ability to induce gephyrin clustering upon overexpression in neurons (Chiou et al., 2011). The human Cb ortholog [also known as human homolog of posterior end mark-2 (PEM2), as well as ARHGEF9] is equivalent to rodent CbIII and also has SH3-containing and SH3-lacking variants (Harvey et al., 2004).

A striking feature of the most abundant Cb variants (i.e. the ones containing SH3 domains) is that their activity is auto-inhibited by interactions of their N-terminal SH3 domain with the DH and PH domains (Soykan et al., 2014). Accordingly, a Cb variant lacking the SH3 domain (ΔSH3-CbII) has an intrinsic gephyrin-clustering activity at the plasma membrane of non-neuronal cells (Kins et al., 2000) and enhances postsynaptic clustering of gephyrin in neurons (Chiou et al., 2011). Instead, Cb variants that carry the SH3 domain [e.g. SH3(+) CbI, SH3(+)CbII or SH3(+)CbIII] are not targeted to the plasma membrane but remain colocalized with intracellular gephyrin deposits (Harvey et al., 2004; Kins et al., 2000). For proper activity, they require additional factors, such as NL2, NL4 (Hoon et al., 2011; Poulopoulos et al., 2009) or the α2-subunit of $GABA_A$Rs (Saiepour et al., 2010), which interact with the Cb SH3 domain and promote an open and active conformation. What is currently still largely unknown is how exactly the various Cb splice variants are differentially employed and regulated during brain development *in vivo*.

The DH domain of Cb calalyses the GDP-GTP exchange on small Rho-like GTPases. Based on biochemical assays with the three best characterized Rho-like GTPases, Cdc42, Rac1 and RhoA, mouse Cb and its human ortholog were initially described as Cdc42-specific GEFs (Reid et al., 1999). However, gephyrin and $GABA_A$R clustering is not affected by forebrain-specific deletion of Cdc42 in mice, indicating that Cb may also activate other Rho-like GTPases in the brain (Reddy-Alla et al., 2010). A likely candidate in this context is TC10 (also known as RhoQ) because it is closely related

[1]Department of Molecular Biology, Universitätsmedizin Göttingen, Humboldtallee 23, Göttingen 37073, Germany. [2]Department of Molecular Neurobiology, Max Planck Institute of Experimental Medicine, Hermann-Rein Str. 3, Göttingen 37075, Germany. [3]MPI-EM Light Microscopy Facility, Max Planck Institute of Experimental Medicine, Hermann-Rein Str. 3, Göttingen 37075, Germany.
*Present address: Hertie Institute for Clinical Brain Research, Center of Neurology, Otfried-Müller-Straße 25, Tübingen 72076, Germany.

‡Author for correspondence (theofilos.papadopoulos@med.uni-goettingen.de)

M.K., 0000-0002-5171-5415; J.H., 0000-0003-1550-3965; T.P., 0000-0002-0684-2407

Received 4 April 2019; Accepted 19 December 2019

Journal of Cell Science (2020) 133, jcs232835. doi:10.1242/jcs.232835

to Cdc42 (Hemsath et al., 2005; Neudauer et al., 1998) and, unlike Cdc42, is fairly specifically expressed in the hippocampus (Tanabe et al., 2000), where the most prominent reduction in gephyrin and $GABA_AR$ clustering occurs upon Cb knockout (Papadopoulos et al., 2007). Indeed, we have previously shown that Cb activates TC10 (Mayer et al., 2013). Moreover, active GTP-TC10 maintains an interaction with the PH domain of Cb as a GTPase-effector complex. This interaction appears to activate Cb as it triggers synaptic gephyrin clustering and enhances GABAergic neurotransmission in cultured hippocampal neurons (Mayer et al., 2013).

While the SH3 domain of Cb controls autoinhibition and activation, the PH domain of Cb is functionally essential. Indeed, deletion of the whole PH domain or PH domain point mutations that abrogate phosphoinosotide binding (Reddy-Alla et al., 2010) abolish Cb-mediated gephyrin clustering in functional assays (Harvey et al., 2004; Reddy-Alla et al., 2010), indicating that phosphoinositide-dependent membrane recruitment is a key step in Cb function. However, information on the postsynaptic roles of phosphoinositides is currently very scarce, which is surprising in view of the well-established roles of phosphoinositides as signalling molecules [e.g. in membrane trafficking, cell compartmentalization (Balla, 2013; Raiborg et al., 2013; Roth, 2004) and presynaptic vesicle recycling and function (Wenk and De Camilli, 2004)].

Phosphatidylinositol 3-phosphate (PI3P) is currently the best validated phosphoinositide ligand of Cb – and the preferred one in multiple experimental contexts (Chiou et al., 2019; Kalscheuer et al., 2009; Papadopoulos et al., 2017, 2015). Recently, for instance, a series of missense mutations in the human Cb gene (R290H, R338W and R356Q) that are linked to epilepsy and intellectual disability were shown to disrupt PI3P binding of Cb and to result in defective gephyrin clustering in neurons (Chiou et al., 2019; Long et al., 2015; Papadopoulos et al., 2015). Moreover, a PI3P pool associated with early/sorting endosomes regulates the postsynaptic clustering of gephyrin and $GABA_ARs$, and hence the strength of inhibitory synapses in cultured neurons (Papadopoulos et al., 2017). While these data nicely illustrate the fact that the PH domain of Cb is employed as a phospholipid-binding domain to regulate synapse maturation, the apparent preference of Cb for PI3P represents a conceptual problem – PI3P is mainly present in early/sorting endosomes (Vicinanza et al., 2008) – which leads to the question as to how Cb can exert its actions at the postsynaptic plasma membrane, where phosphoinositides such as $PI(3,4)P_2$, $PI(4,5)P_2$, and $PI(3,4,5)P_3$ are abundant (Vicinanza et al., 2008).

In the present study, we addressed this problem, focusing on the TC10–Cb interaction (Mayer et al., 2013). We show that a polybasic stretch in the C-terminus of TC10 is required for binding of TC10 to monophosphorylated phosphoinositides, and that the interaction of TC10 with phospholipids via this polybasic stretch is essential for the TC10-triggered induction of Cb-mediated clustering of gephyrin. Most importantly, we provide evidence that TC10 binding switches the phospholipid preference of Cb, allowing it to specifically interact with phosphoinositides enriched at the plasma membrane in order to trigger postsynaptic gephyrin clustering.

RESULTS

A polybasic stretch in the C-terminus of TC10 is important for Cb-dependent gephyrin microcluster formation

Our previously published work (Mayer et al., 2013), showed that TC10 stimulates Cb-dependent gephyrin clustering by binding, in its active, GTP-bound state, to the PH domain of Cb. These previous data indicated that GTP-TC10 activates Cb by relieving autoinhibition. However, the molecular mechanisms through which TC10 achieves this, as well as in which subcellular compartments the interaction between GTP-TC10 and Cb takes place remain unclear.

Small GTPases have unique functions at specific compartments and hence their subcellular localization is an important regulatory mechanism (Liu et al., 2012). A key determinant of the intracellular distribution of GTPases is their C-terminal hypervariable region, which can contain diverse types of subcellular localization signals. Similar to what is seen in most Rho family GTPases, the C-terminus of TC10 terminates in a CaaX motif (CLIT; Fig. 1A) and C210 of TC10 is a target of farnesylation (boxed in Fig. 1A; Roberts et al., 2008). Furthermore, there are two additional cysteine residues (underlined) in the C-terminus of TC10 that can be palmitoylated. Palmytoylation is thought to prevent the solubilization of membrane-bound TC10 by RhoGDI and to assure the localization in a lipid microdomain (Michaelson et al., 2001; Murphy et al., 2001; Watson et al., 2003). In addition, TC10 has a polybasic stretch (residues coloured red in Fig. 1A) in its C-terminus.

In order to dissect the role of the TC10 C-terminus in Cb-dependent gephyrin clustering, we employed a previously described cell-based assay (Mayer et al., 2013; Papadopoulos et al., 2015). Briefly, COS-7 cells coexpressing TC10 together with GFP–gephyrin and the autoinhibited splice variant of Cb, which contains an N-terminal SH3 domain [SH3(+)CbII], have a singificantly increased percentage of GFP–gephyrin that is redistributed into submembranous microclusters, as compared to cells expressing GFP–gephyrin and SH3(+)CbII in the absence of TC10 (Fig. 1B; Fig. S1). The increased GFP–gephyrin microcluster formation in the presence of TC10 is due to an interaction of the PH domain of Cb with the GTP-loaded GTPase, which relieves the autoinhibition of Cb (Mayer et al., 2013; Soykan et al., 2014). We first analysed the ability of chimeric constructs to induce Cb-mediated formation of GFP–gephyrin microclusters, in which the C-terminus of TC10 was exchanged for the one from H-Ras or K-Ras, respectively, as was previously described (Watson et al., 2001). The C-termini of all three GTPases contain a CaaX box (Fig. 1A). Both, TC10 and H-Ras have a dual palmitoylation site, while TC10 and K-Ras share a polybasic stretch (Fig. 1A). In our cell-based assay, only 34.9 ±5.8% of cells coexpressing HA–TC10 H-Ras and 21.6±4.3% (mean±s.e.m.) of cells coexpressing HA–TC10 K-Ras, together with GFP–gephyrin and SH3(+)CbII, showed microclusters, as compared to control cells coexpressing wild-type HA–TC10 (HA–TC10 WT). This indicates that the C-terminus of TC10 is important for mediating Cb-dependent formation of submembranous GFP–gephyrin microclusters. Neither a similar pattern of palmitoylation, as found in H-Ras, nor an alternative polybasic stretch, as that of K-Ras, was sufficient to induce GFP–gephyrin microcluster formation to a similar degree to that observed for cells coexpressing TC10 WT (Fig. 1B; Fig. S1).

We therefore performed a more-detailed analysis of the different functional elements of the TC10 C-terminus to unravel the contributions of prenylation, palmitoylation and the polybasic residues to Cb-dependent gephyrin microcluster formation. In order to study the importance of membrane anchoring of TC10 by prenylation, we mutated the cysteine residue of the CaaX motif (C210S; boxed in Fig. 1A). This mutation leads to a cytosolic distribution of the protein (Watson et al., 2003). The C210S mutation significantly impaired the ability of TC10 to induce Cb-mediated formation of GFP–gephyrin microclusters, indicating the importance of the prenylation for the proper function of the GTPase, as noted previously (Winter-Vann and Casey, 2005). A second,

Journal of Cell Science (2020) 133, jcs232835. doi:10.1242/jcs.232835

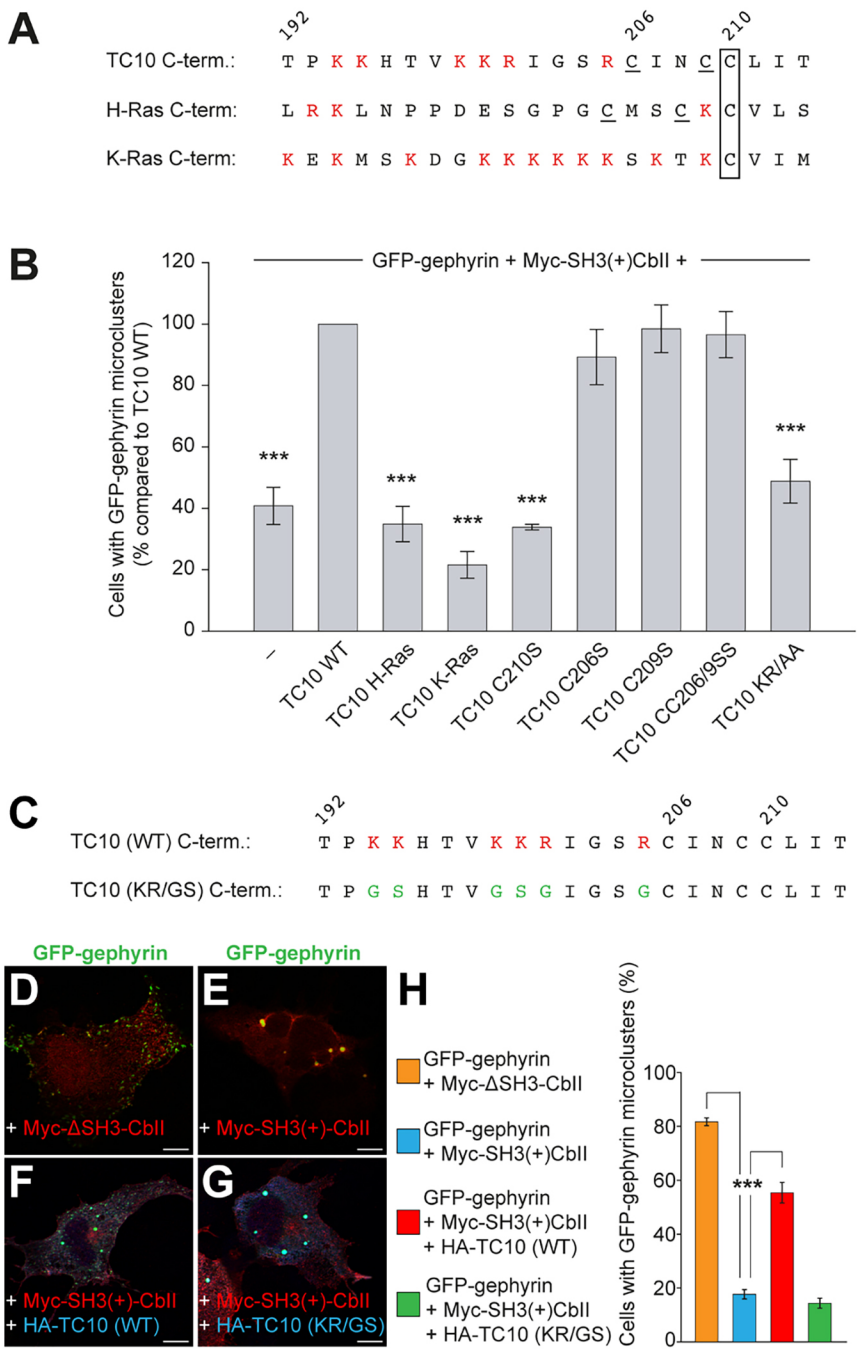

Fig. 1. The C-terminal basic residues of TC10 are important for Cb-dependent formation of gephyrin microclusters. (A) Alignment of the last 22 amino acids of the Rho family GTPase TC10 and the Ras family GTPases H-Ras and K-Ras. Basic residues are highlighted in red, palmitoylated cysteine residues are underlined and prenylated cysteine residues are boxed. (B) Quantification of the percentage of COS7 cells co-transfected with GFP–gephyrin and Myc–SH3(+)CbII in the presence or absence of HA–TC10 mutants classified as having GFP–gephyrin microclusters. Values were normalized to the level of GFP–gephyrin microclusters in cells transfected with GFP–gephyrin, Myc–SH3(+)CbII and HA–TC10 WT. Results are means±s.e.m. of N=3 independent transfections and n=348-630 cells per transfection condition. ***P<0.001 compared to cells transfected with GFP–gephyrin, Myc–SH3(+)CbII and HA–TC10 WT (set at 100%, second bar) [one-way ANOVA, F (8,18)=31.66, P<0.0001, followed by a Tukey multiple comparison test]. (C) Alignment of the last 22 C-terminal amino acids of TC10 WT and the TC10 KR/GS mutant. Mutated residues are highlighted in green. (D–G) COS7 cells transfected as indicated showing GFP–gephyrin microclusters or aggregates. Scale bars: 10 µm. (H) The percentage of transfected cells as indicated that are classified as displaying GFP–gephyrin microclusters. Data represent means±s.e.m. of N=3 independent experiments and n=300 cells. ***P<0.001 compared to cells transfected only with GFP–gephyrin and Myc–SH3(+)CbII (second bar) [one-way ANOVA, F (3,8)=176.8, P<0.0001, followed by a Tukey multiple comparison test].

reversible mode of membrane attachment is the palmitoylation of TC10 at two cystein residues (C206 and C209; underlined in Fig. 1A; Michaelson et al., 2001; Roberts et al., 2008). However, mutating one (C206S or C209S) or both (CC206/9SS) of the palmitoylated cysteine residues did not affect TC10-triggered Cb-dependent gephyrin clustering, as compared to controls (Fig. 1B; Fig. S1).

Having excluded a major role of palmytoylation of TC10 in triggering Cb-mediated distribution of GFP–gephyrin into submembraneous microclusters, we investigated the role of C-terminal polybasic stretch of TC10, which that can potentially interact with negatively charged amino acids or membrane lipids. In order to determine the contribution of the basic residues to TC10 function in gephyrin clustering, we initially replaced all lysine (K) and arginine (R) residues (highlighted in red in Fig. 1A) by alanine (A) residues (denoted as TC10 KR/AA in Fig. 1B; Fig. S1). The TC10 KR/AA mutant could not trigger the formation of Cb-dependent GFP–gephyrin microclusters in COS-7 cells. Only 48.8±7.1% of cells displayed GFP–gephyrin microclusters, as compared to controls coexpressing TC10 WT (Fig. 1B). This result is not significantly different from that obtained with cells coexpressing GFP–gephyrin and SH3(+)CbII in the absence of TC10 (first column in Fig. 1B; 40.79±6.03%). In addition, the basic K and R C-terminal residues of TC10 were replaced by glycine (G) and serine (S) residues (Fig. 1C). Based on the observation that in the C-terminus of H-Ras (which in contrast to K-Ras lacks a polybasic stretch), glycine and serine residues are frequent, the alternative KR/GS mutations in the C-terminus of TC10 (Fig. 1C) are considered as closer to naturally

Journal of Cell Science (2020) 133, jcs232835. doi:10.1242/jcs.232835

occurring substitutions within the family of small Rho-like GTPases. Again, we coexpressed Myc-tagged CbII splice variants with or without an N-terminal SH3 domain [SH3(+)CbII and ΔSH3-CbII, respectively; Fig. 1D,E] together with GFP–gephyrin in COS-7 cells. As described previously (Harvey et al., 2004; Kins et al., 2000), in the majority of double-transfected cells, the constitutively active splice-variant ΔSH3-CbII, but not the autoinhibited splice-variant SH3(+)CbII, induced the formation of GFP–gephyrin microclusters (>50 GFP–gephyrin-positive puncta per cell; Fig. 1D,E). Hence, the percentage of transfected cells displaying microclusters was strongly reduced in cells expressing SH3(+)CbII, as compared to those expressing the constitutively active ΔSH3-CbII isoform (17.67±1.76% versus 81.67±1.45%, respectively; mean±s.e.m.; Fig. 1H). As shown previously (Mayer et al., 2013), HA–TC10 WT relieves autoinhibition of SH3(+)CbII and enhances SH3(+)CbII-mediated gephyrin clustering (Fig. 1F). The fraction of cells displaying GFP–gephyrin microclusters was significantly higher in the presence of TC10 WT (55.33±3.84%), as compared to cells expressing only GFP–gephyrin and SH3(+)CbII (Fig. 1H). In contrast, the HA–TC10 KR/GS mutant failed to trigger the formation of gephyrin microclusters (Fig. 1G). Accordingly, the fraction of cells displaying GFP–gephyrin microclusters was not significantly different to those coexpressing only GFP–gephyrin and SH3(+)CbII (14.33±1.85%; Fig. 1H). These results are in line with the results obtained with the corresponding TC10 KR/AA mutant (Fig. 1B) and indicate an important role for the C-terminus of TC10 in the mechanism regulating Cb-mediated gephyrin microcluster formation.

The TC10 KR/GS mutant fails to stimulate perisomatic clustering of gephyrin in cultured hippocampal neurons

Our previous study indicated that TC10 overexpression enhances the clustering of endogenous gephyrin in dissociated rat hippocampal neurons, particularly at perisomatic sites (Mayer et al., 2013). In order to analyse whether this function of TC10 is retained in the TC10 KR/GS mutant, we transfected cultured hippocampal neurons at days *in vitro* (DIV) 4 with HA–TC10 WT or the HA–TC10 KR/GS mutant, or left them untransfected (Fig. 2A–C). In order to analyse clustering of gephyrin at nascent synapses, cells were fixed at DIV 9 and stained with antibodies against gephyrin, vesicular inhibitory amino acid transporter (VIAAT, also known as SLC32A1) and the HA tag (Fig. 2A–C). In agreement with our previous study (Mayer et al., 2013), overexpression of TC10 WT led to an increase in the density and size of perisomatic gephyrin clusters (Fig. 2D,E). In contrast, no statistical differences between groups were obtained for dendritic immunoreactivities (Fig. 2G–I), as compared to untransfected cells. The TC10 KR/GS mutant lacked this stimulatory activity at perisomatic synapses, as compared to control cells (Fig. 2D,E). Quantifications of the densities of VIAAT immunoreactive puncta on the perisomatic and dendritic regions of the analysed neurons revealed no significant differences between groups (Fig. 2F,I), indicating that the numbers of inhibitory nerve terminals were not changed upon TC10 overexpression. These results indicate that the basic amino acids in the C-terminus of TC10 are essential for the ability of this GTPase to induce enhanced clustering of neuronal gephyrin at perisomatic synapses.

The KR/GS mutation does not affect the binding of active TC10 to Cb

The interaction sites involved in the interaction between active, GTP-loaded TC10 and the DH-PH tandem domain of Cb (Mayer et al., 2013) have not yet been characterized in detail. This prompted us to test whether the KR/GS mutation affects the properties of Cb binding by GTP-loaded TC10. To this end, we performed *in vitro* binding assays, using purified GTPγS-loaded TC10 (WT or the KR/GS mutant) and purified glutathione-S-transferase (GST)-tagged ΔSH3-CbII (GST–ΔSH3-CbII), as described previously (Mayer et al., 2013; Papadopoulos et al., 2015). Notably, GTPγS-TC10 KR/GS also bound to Cb (Fig. S2A) and exhibited WT-like binding efficacy (Fig. S2B). Control incubations with GST alone instead of GST–ΔSH3-CbII confirmed the specificity of the binding (Fig. S2A). These results indicate that the KR/GS mutation does not affect the interaction of active TC10 with the non-catalytic site in the DH/PH-tandem domain of Cb.

The KR/GS mutation impairs binding of TC10 to monophosphorylated phosphoinositides

Protein surfaces that interact with phosphoinositides consist of clusters of basic residues (for a review, see Di Paolo and De Camilli, 2006). Most Rho GTPases contain a cluster of positively charged residues directly preceding their geranylgeranyl moiety. This suggests that interactions of small GTPases with membrane-bound phosphoinositides might contribute to their positioning at the appropriate cellular membrane sites for signal propagation. Thus, we aimed to investigate whether TC10 binds to phosphoinositides through its C-terminal polybasic sequence. To this end, we used immobilized phosphoinositides (Fig. 3A) and tested the ability of recombinant TC10 or the respective TC10 KR/GS mutant that were preloaded with either GDP or GTPγS to interact with the indicated phosphoinositides in a protein-lipid overlay assay as described previously (Papadopoulos et al., 2015). The results indicated that both GDP- and GTPγS-loaded TC10 associate mainly with monophosphorylated phosphoinositides (PI3P, PI4P and PI5P; Fig. 3A). In contrast, the binding of GDP-loaded TC10 KR/GS and GTPγS-loaded TC10 KR/GS to monosphosphorylated phosphoinositides was strongly reduced as compared to what was seen for the corresponding WT proteins (Fig. 3A). These data provide the first evidence that the basic amino acids in the C-terminus of TC10 are essential for the ability of this GTPase to preferentially interact with certain phosphoinositides.

Since the nucleotide-bound state of TC10 did not affect the binding of this GTPase to monosphosphorylated phosphoinositides, we used the GTPγS-loaded state of the GTPase in all subsequent experiments. This was motivated by our previous finding that Cb interacts preferentially with active, GTP-loaded, TC10 (Mayer et al., 2013). Furthermore, previous studies have shown that the SH3 domain-containing Cb isoform does not bind to phosphoinositides due to its more closed conformation, as compared to the isoform lacking the SH3 domain (Soykan et al., 2014), which interacts preferentially with monophosphorylated phosphoinositides (Fig. S2 and Soykan et al., 2014). In agreement with our previous studies (Soykan et al., 2014) our protein-lipid overlay assays disclosed that GST–SH3(+)CbII alone is not capable of interacting with phosphoinositides (Fig. 3B). In the presence of both GST–SH3(+)CbII and GTPγS-loaded TC10, the interaction of TC10 WT, but not that of the TC10 KR/GS mutant with monophosphorylated phosphoinositides was stronger, as compared to the immunoreactive signal obtained with membranes that had been incubated with GTPγS-TC10 alone (Fig. 3B). Subsequently, we incubated the same membranes with a GST-specific antibody, which allowed us to visualize the binding of GST–SH3(+)CbII to certain phosphoinositides (Fig. 3B). A prominent interaction of GST–SH3(+)CbII with PI(4,5)P_2, and to

Journal of Cell Science (2020) 133, jcs232835. doi:10.1242/jcs.232835

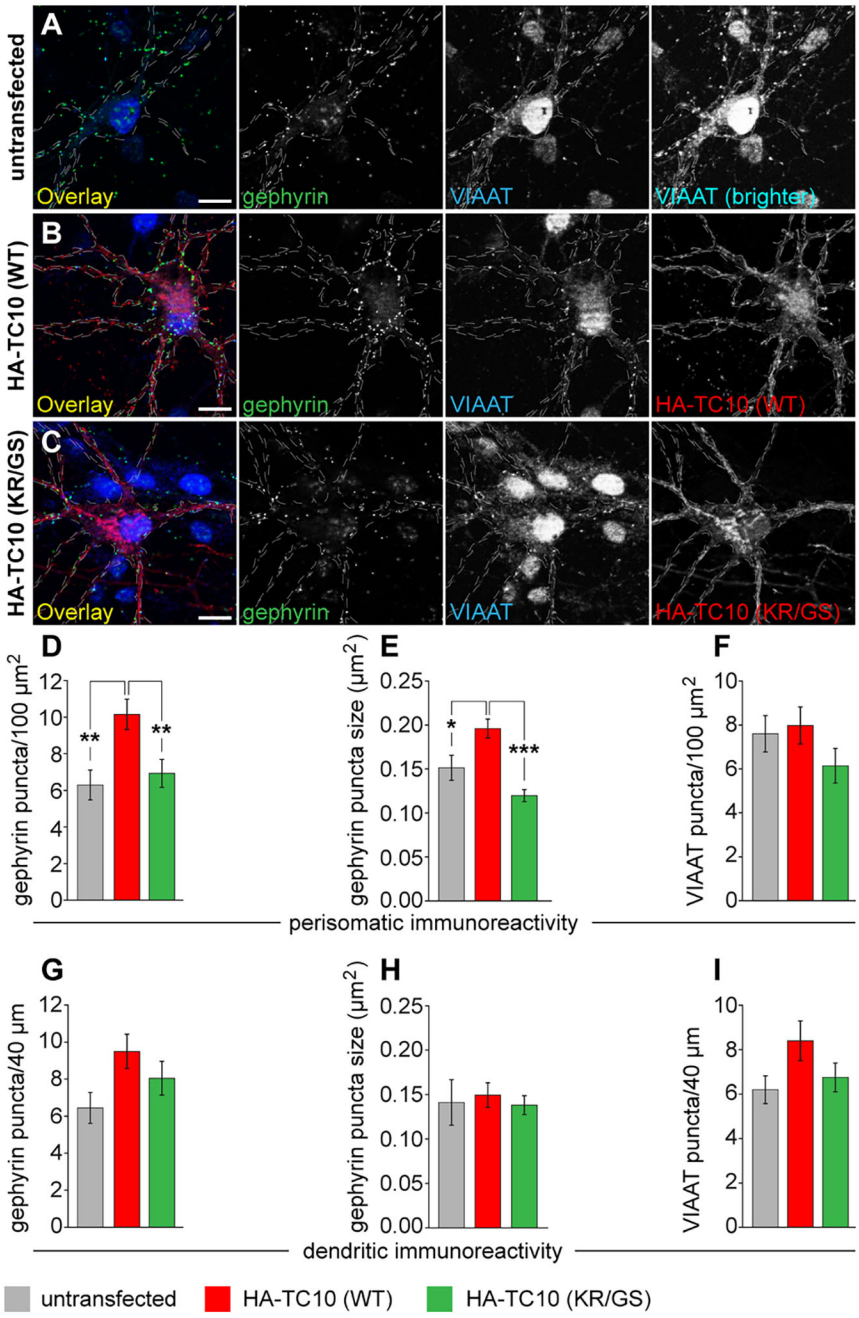

Fig. 2. The C-terminal basic residues of TC10 are important for the perisomatic clustering of gephyrin in cultured hippocampal neurons. (A–C) Cultured rat hippocampal neurons were transfected at DIV 4 as indicated. Untransfected neurons (A) served as a control. At DIV 9, neurons were fixed and immunostained for gephyrin (green), HA (red) and VIAAT (blue). Particular neurons (indicated by dotted lines) were identified by either increasing the brightness of the VIAAT staining in images of untransfected cells (A; right panel) or tracing the HA staining of transfected neurons (B,C; right panels). Scale bars: 10 µm. (D–F) Bar graphs of perisomatic gephyrin (D) or VIAAT (F) cluster densities per 100 µm^2 surface area and perisomatic gephyrin cluster sizes (L), as indicated. Bars correspond to counts on perisomatic surface areas of 20 individual neurons per condition (D,F) and 156–432 individual clusters (E) from three independent transfection experiments. (G–I) Bar graphs of gephyrin (G) or VIAAT (I) cluster densities and gephyrin cluster sizes (H) in 40 µm second-order dendrites, as indicated. Bars correspond to counts on dendrites of 20 individual neurons (G,I) and 129–190 individual clusters (H) from three independent transfection experiments. Data represent mean±s.e.m. **P*<0.05, ***P*<0.01, ****P*<0.001 [one-way ANOVA, D, *F* (2, 57)=6.646, *P*=0.0025; E, *F*(2, 57)=12.06, *P*<0.0001; F, *F*(2, 57)=1.396, *P*=0.2558; G, *F* (2, 57)=2.932, *P*=0.0614; H, *F*(2, 57)=0.2293, *P*=0.7958; I, *F*(2, 57)=2.443, *P*=0.0960. Multiple comparison was performed using the Tukey test].

a lesser extent with PI(3,4,5)P_3, in the presence of GTPγS-TC10 (WT or KR/GS) was also observed with membranes that have been exclusively incubated with a GST-specific antibody (Fig. S3). These data indicate that the interaction of Cb with the small GTPase TC10 enhances the affinity of the Cb–TC10 complex for certain phosphoinositides.

The KR/GS mutation affects the localization of TC10 or Cb–TC10 complexes on early/sorting endosomes

TC10 is localized both at the plasma membrane and in endomembrane compartments (Watson et al., 2003). The preferential interaction of TC10 with monophosphorylated phosphoinositides, particularly PI3P, and the impairment of this interaction in the KR/GS mutant prompted us to investigate further whether TC10 is localized on PI3P-containing endosomes. To address this, we co-transfected NIH-3T3 cells with mCherry-tagged Rab5 together with either HA–TC10 WT or the HA–TC10 KR/GS mutant in the absence (Fig. 4A–L) or in the presence (Fig. S4) of Myc–SH3(+)-CbII. Rab5 (herein referring to the Rab5a form) is the most extensively analysed Rab of the early endocytic pathway and is considered a specific marker of the PI3P-rich early/sorting endosomes (Christoforidis et al., 1999; Murray et al., 2002; Schwartz et al., 2007). In the absence of highly specific antibodies for confocal microscopy of endogenous Rab5, low expression of a recombinant GTPase, as performed in this study (see Materials and Methods) has been widely used and contributed to the characterization of its subcellular localization (Schwartz et al., 2007). In cells expressing HA–TC10 WT (Fig. 4A–F; Fig. S4), enriched HA immunoreactivity was observed in mCherry–Rab5-positive endosomes (see exemplary closed circles in Fig. 4D–F), as compared to the immunoreactive signal in extraendosomal areas (exemplary dashed circles in Fig. 4D–F and Fig. S4). In contrast, in

Journal of Cell Science (2020) 133, jcs232835. doi:10.1242/jcs.232835

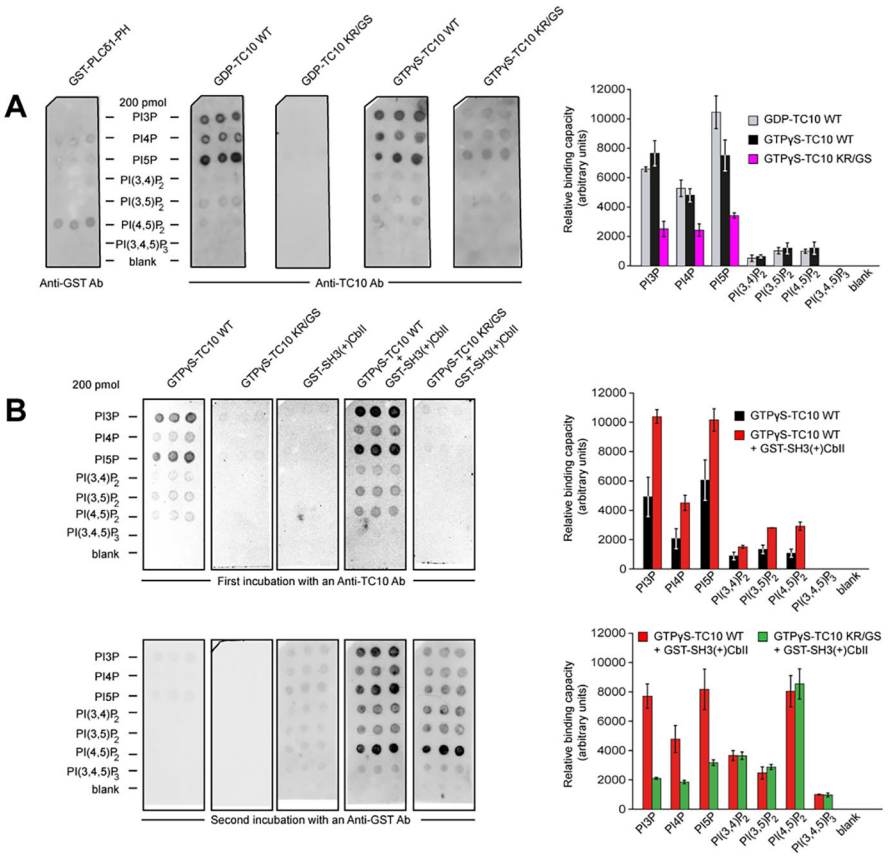

Fig. 3. The C-terminal basic residues of TC10 are important for TC10 binding to monophosphorylated phosphoinositides. (A) Protein-lipid overlay assays using 0.5 µg/ml (total amount 2.5 µg) of proteins as indicated on the top of the membranes. Phosphoinositides (Echelon, PInPs-diC16) were spotted onto the Hybond-C-extra membranes (GE Healthcare), as indicated. GST–PLCδ1-PH was used to confirm the specificity of the assay. Right panel, relative phosphoinositide-binding capacities of TC10 WT and the KR/GS-mutant, as indicated, determined by measuring the intensity of the chemiluminescence. The data represent means ±s.e.m. of *n*=3 measurements. (B) Protein-lipid overlay assays using GTPγS-TC10 WT, GTPγS-TC10 KR/GS or GST–SH3(+)CbII, either alone or in a 1:1 ratio, as indicated. Top, interactions with the different phosphoinositides were detected by incubating the membranes with a TC10-specific antibody. Bottom, subsequently, the same membranes were extensively washed and incubated with a goat anti-GST–HRP conjugate antibody for detecting GST–SH3(+)CbII-specific immunoreactivities. Right panels, relative phosphoinositide-binding capacities of proteins, as indicated, determined by measuring the intensity of the chemiluminescence. The data represent means ±s.e.m. of *n*=3 measurements. Left panels in A, B show representative immunoreactive signals of *n*=3 independent experiments.

cells expressing the HA–TC10 KR/GS mutant alone (Fig. 4G–L) the HA immunoreactive signal was not higher in mCherry–Rab5-labelled endosomes as compared to extraendosomal areas. Furthermore, the endosomal localizations of both HA–TC10 KR/GS and Myc–SH3(+)-CbII were significantly reduced as compared to what was found for control cells coexpressing Myc–SH3(+)-CbII together with HA–TC10 WT (Fig. S4). In addition, fluorescence intensity plot analysis (Fig. 4M,N; Fig. S4) indicated enhanced accumulation of HA–TC10 WT (Fig. 4M and Fig. S4) as compared to the HA–TC10 KR/GS (Fig. 4N and Fig. S4) immunoreactivity in mCherry–Rab5-positive endosomes. Quantitative analysis of the ratios of the mean grey values in endosomal areas (see exemplary closed circles in Fig. 4D,E,J,K and Fig. S4) to the mean grey values in adjacent and equivalent extraendosomal areas (see exemplary dashed circles in Fig. 4D,E,J,K and Fig. S4) indicated significantly increased values in cells expressing HA–TC10 WT, as compared to those expressing the HA–TC10 KR/GS mutant (Fig. 4O; in the absence of Cb, WT ratio of 1.34±0.038 versus KR/GS ratio of 1.09 ±0.015; Fig. S4, in the presence of Cb, WT ratio of 1.92±0.09 versus a KR/GS ratio of 1.59±0.07; mean±s.e.m.). Similarly, the endosomal localization of Myc–SH3(+)-CbII in the presence of HA–TC10 WT (Fig. S4; ratio 3.14±0.32) was significantly increased, as compared to that in the presence of the HA–TC10 KR/GS mutant (Fig. S4; ratio 2.37±0.19). These results indicate that the KR/GS mutation significantly affects the localization of TC10 or TC10–Cb complexes on PI3P-containing early/sorting endosomes.

TC10 induces a phosphoinositide affinity switch on Cb

In our protein-lipid overlay assays, the phosphoinositides were not embedded in a lipid membrane. The resulting different presentation of the phosphorylated headgroup positions may affect binding specificities. To quantitatively compare binding affinities of GTPγS-TC10 (WT or KR/GS) to phosphoinositide-containing lipid membranes in the absence or presence of GST–SH3(+)CbII we used a surface plasmon resonance (SPR) approach, a system that reflects the situation in live cells more closely. To this aim, we injected different concentrations of the proteins (see Materials and Methods and legend to Fig. 5) over the surface of an SPR sensor chip coated with vesicles containing the indicated phosphoinositides (Fig. 5), and determined the equilibrium binding constants for interactions measured between different phosphoinositides and GTPγS-TC10 (WT or KR/GS), GST–SH3(+)CbII or the respective stoichiometric mixtures of GTPase and Cb (Fig. 5). The affinity binding constants (Table 1) for interactions measured between indicated proteins and phosphoinositides were determined as described in the Materials and Methods. Comparison of the affinity binding constants indicated that the KR/GS mutation significantly decreased the ability of TC10 to bind to all phosphoinositides tested (Table 1). Since SH3(+)CbII forms a closed and autoinhibited conformation where the SH3 domain interacts with the DH-PH tandem domain (Soykan et al., 2014) we further analysed the binding of GST–SH3(+)CbII to vesicles containing the indicated phosphoinositides. In agreement with previous studies (Ludolphs et al., 2016; Soykan et al., 2014), the obtained affinity binding constants (Table 1) indicate that only a minor fraction of GST–SH3(+)CbII is capable of binding to phosphoinositide-containing lipid membranes. In contrast, when stoichiometric mixtures of GST–SH3(+)CbII with GTPγS-TC10 WT or GTPγS-TC10 KR/GS were injected, a significant increase in the binding affinities of the protein complexes was observed for PI3P, $PI(4,5)P_2$ and $PI(3,4,5)P_3$ (Table 1, Fig. 5). As both the TC10 WT and the KR/GS mutant

Journal of Cell Science (2020) 133, jcs232835. doi:10.1242/jcs.232835

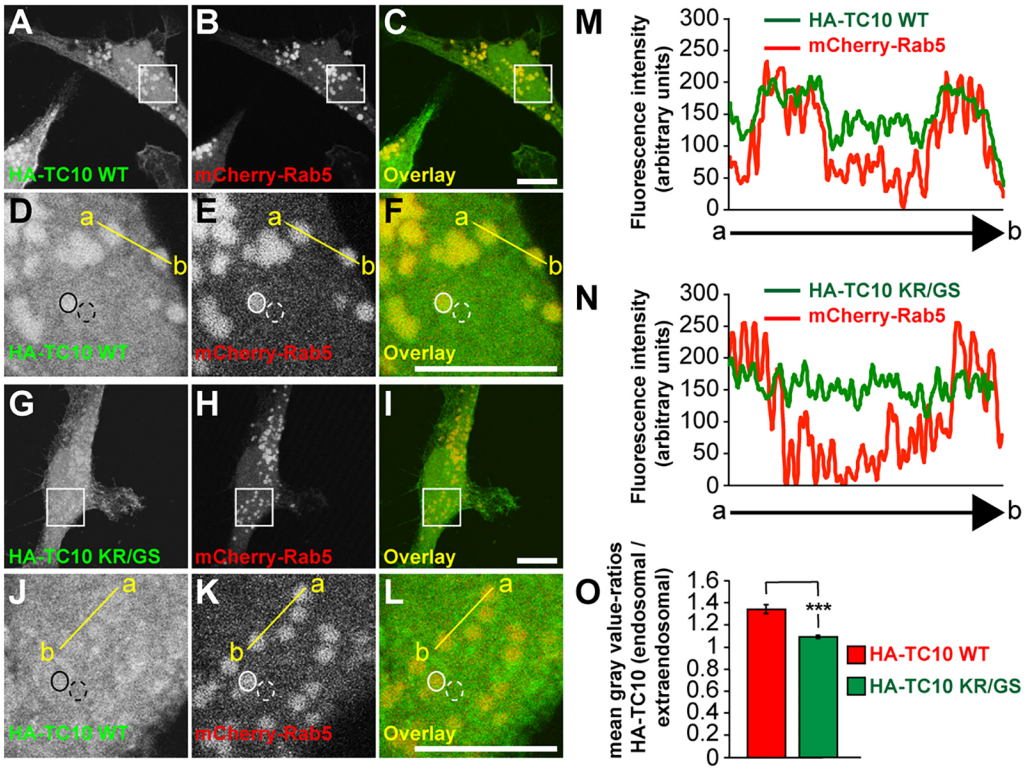

Fig. 4. The KR/GS mutation affects the localization of TC10 at mCherry–Rab5-labelled endosomes. (A–L) NIH-3T3 cells coexpressing HA–TC10 WT (A–F) or the HA–TC10 KR/GS mutant (G–L) together with mCherry–Rab5, as indicated. (D–F,J–L). Magnifications of the boxed areas in A–C and G–I, respectively. Scale bars: 10 µm. (M,N) Fluorescence intensity scans over the yellow lines in F (M, HA–TC10 WT, green; N, HA–TC10 KR/GS, green) and L (M,N: mCherry–Rab5, red), respectively. (O) For statistical comparison, the following the value for mean grey values of endosomal HA–TC10/mean grey values of extraendosomal HA–TC10 [WT (red) or the KR/GS mutant (green)] was calculated. Endosomal (closed circles) and extraendosomal (dashed circles) areas were preselected as exemplary indicated by the closed and dashed circles in E and K, respectively. For each cell, the mean grey values of at least ten endosomal and ten extraendosomal areas were calculated. The data represent means±s.e.m. ***P<0.001 (unpaired two-tailed Student's t-test) of N=3 independent experiments and n=20 cells per condition.

induced an increase in the binding affinities of the Cb–TC10 complexes for PI3P, PI(4,5)P_2 and PI(3,4,5)P_3, we propose that the binding of TC10 to Cb induces a conformational switch that allows for selective interaction of the Cb–TC10 complex with those three phosphoinositides (Table 1, Fig. 5). In line with this interpretation, injecting stoichiometric mixtures of GST–SH3(+)CbII with GTPγS-TC10 WT does not significantly increase the binding affinity of the Cb–TC10 complex to PI5P, as compared to the affinity obtained with GTPγS-TC10 WT alone (Table 1, Fig. 5). Furthermore, the low binding affinity for PI5P obtained by injecting stoichiometric mixtures of GST–SH3(+)CbII with GTPγS-TC10 KR/GS (Table 1, Fig. 5) indicates that binding of TC10 to Cb does not just lead to an unspecific increase in the binding affinities of the Cb–TC10 complex for all phosphoinositides. Thus, in line with our results obtained with the protein-lipid overlay assays, our SPR measurements indicate a specific switching in the affinity of the Cb–TC10 complex towards certain phosphoinositides, such as PI3P, PI(4,5)P_2 and PI(3,4,5)P_3.

PI(4,5)P_2 at the plasma membrane is important for Cb-mediated gephyrin clustering

Recently, we identified a pool of PI3P associated with early/sorting endosomes to be a critical regulator of postsynaptic gephyrin and $GABA_AR$ clustering (Papadopoulos et al., 2017). However, one critical issue arising from previous studies was that PI3P, the best-characterized Cb ligand so far (Chiou et al., 2019; Kalscheuer et al., 2009; Papadopoulos et al., 2015; Reddy-Alla et al., 2010), is mainly concentrated in membranes of early/sorting endosomes (for a review, see Vicinanza et al., 2008). Thus, it was difficult to understand how this phosphoinositide contributes to the clustering of gephyrin at the plasma membrane. Our results obtained with the protein-lipid overlay assays and our SPR analyses of Cb–TC10-complexes reveal the relevance of additional phosphoinositides, such as PI(4,5)P_2 and PI(3,4,5)P_3, in TC10-induced Cb-mediated clustering of gephyrin at the plasma membrane. To more precisely define the importance of these phosphoinositides for gephyrin clustering at the plasma membrane, the following approach was used.

We used a stable HEK 293 cell line (Flp-In-T-Rex-EGFP-gephyrin HEK 293), which inducibly expresses EGFP–gephyrin upon addition of tetracycline (TET) to the culture medium (Papadopoulos et al., 2017). TET induction for ∼4 h leads to the formation of large intracellular EGFP–gephyrin aggregates, whereas coexpression of the constitutively active Cb isoform ΔSH3-CbII redistributes these aggregates into submembraneous microclusters owing to the ability of ΔSH3-CbII to simultaneously bind gephyrin and membrane lipids (Papadopoulos et al., 2017; Soykan et al., 2014). In order to study the importance of PI3P, PI(4,5)P_2 or PI(3,4,5)P_3 for Cb-mediated plasma membrane recruitment of newly synthesized EGFP–gephyrin, we used the Flp-In-T-Rex-EGFP-gephyrin HEK 293 cell line in combination with a previously published rapidly reversible chemical dimerizer (rCD1) system (Feng et al., 2014). The rCD1-based system (see schematic representation in Fig. S5 and Fig. 6A) allows the targeting

Journal of Cell Science (2020) 133, jcs232835. doi:10.1242/jcs.232835

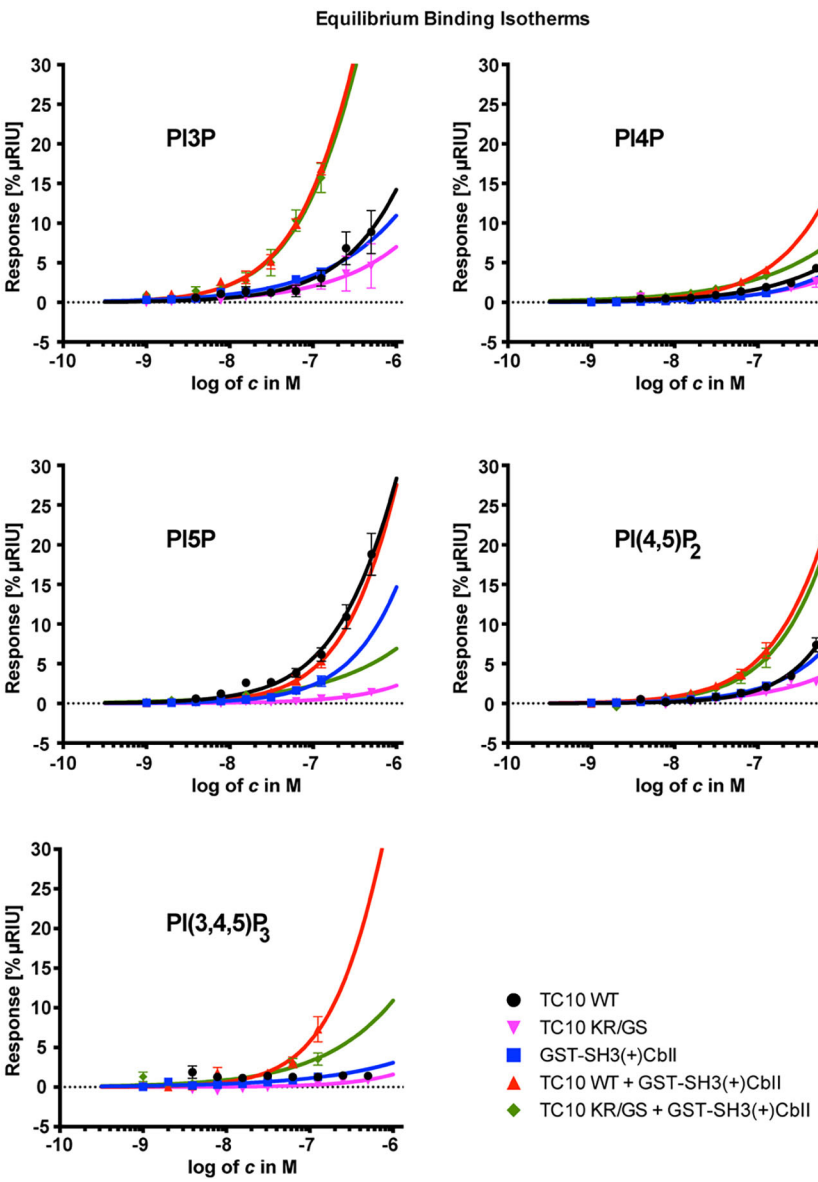

Fig. 5. TC10 acts as a specificity regulator of Cb-binding to certain phosphoinositides. (A–E) Equilibrium binding isotherms for interactions between the indicated phosphoinositides and TC10 WT, TC10 KR/GS, GST–SH3(+)CbII or the respective stoichiometric mixtures of TC10 WT or TC10 KR/GS with GST–SH3(+)CbII, as indicated. TC10 and TC10 KR/GS were initially loaded with GTPγS. Proteins were serially diluted and injected over the surface of an SPR sensor chip coated with vesicles containing the phosphoinositides, as described in the Materials and Methods. The obtained response was normalized and plotted against the concentration (*c* in M, displayed in a logarithmic scale). RIU, refractive index units. The data represent means±s.e.m. of at least three independent experiments.

of a given active enzyme to a defined subcellular compartment by adding rCD1, which leads to rapid dimerization based on two standard protein fusions, the FK506-binding protein (FKBP) and SNAP tag (Feng et al., 2014). In a second step, the translocated enzyme is rapidly removed by addition of a commercially available competing ligand [FK506; (Feng et al., 2014); also see the schematic representation in Fig. 6A]. In our approach (Fig. 6A and Fig. S5), the system permitted the rCD1-mediated accumulation of defined phosphoinositide-phosphatases as mRFP–FKBP fusion proteins [Myotubularin 1 (MTM1) for PI3P; PI5-Ptase for $PI(4,5)P_2$ and PTEN for $PI(3,4,5)P_3$] to the plasma membrane through dimerization with the plasma-membrane-associated ECFP–Lck–SNAP (Feng et al., 2014). Before the application of rCD1, while ECFP–Lck–SNAP resided at the plasma membrane, mRFP–FKBP alone (control) and the mRFP–FKBP-fused phosphoinositide phosphatases MTM1, PI5-Ptase and PTEN were evenly distributed in the cytoplasm and nucleus (Fig. S5, left). As described previously (Feng et al., 2014), addition of 1 µM rCD1 induced translocation of the mRFP–FKBP fusion proteins to the plasma membrane (Fig. S5, right). In Flp-In-T-Rex-EGFP-gephyrin HEK 293 cells co-transfected with Myc–ΔSH3-CbII (unstained), ECFP–Lck–SNAP (blue) and the different mRFP–FKBP fusion

Table 1. Affinity binding constants obtained for interactions measured between indicated proteins and phosphoinositides

	TC10 WT	TC10 KR/GS	GST–SH3(+)CbII	TC10 WT+GST–SH3(+)CbII	TC10 KR/GS+GST–SH3(+)CbII
PI3P	11.80±2.38	103.51±8.14	49.20±7.90	0.81±0.26	0.90±0.27
PI4P	124.45±25.47	330.37±34.73	79.98±10.70	7.93±2.08	128.82±15.48
PI5P	3.12±0.93	181.55±36.58	7.83±1.36	2.86±0.70	176.60±27.24
$PI(4,5)P_2$	7.69±2.26	212.81±30.12	22.08±4.82	3.03±0.77	3.50±0.73
$PI(3,4,5)P_3$	–	–	2275.10±119.33	1.74±0.39	41.40±4.70

Affinity binding constants as K_D (µM). The data represent means±s.e.m. of at least three independent experiments. –: no detectable binding.

Journal of Cell Science (2020) 133, jcs232835. doi:10.1242/jcs.232835

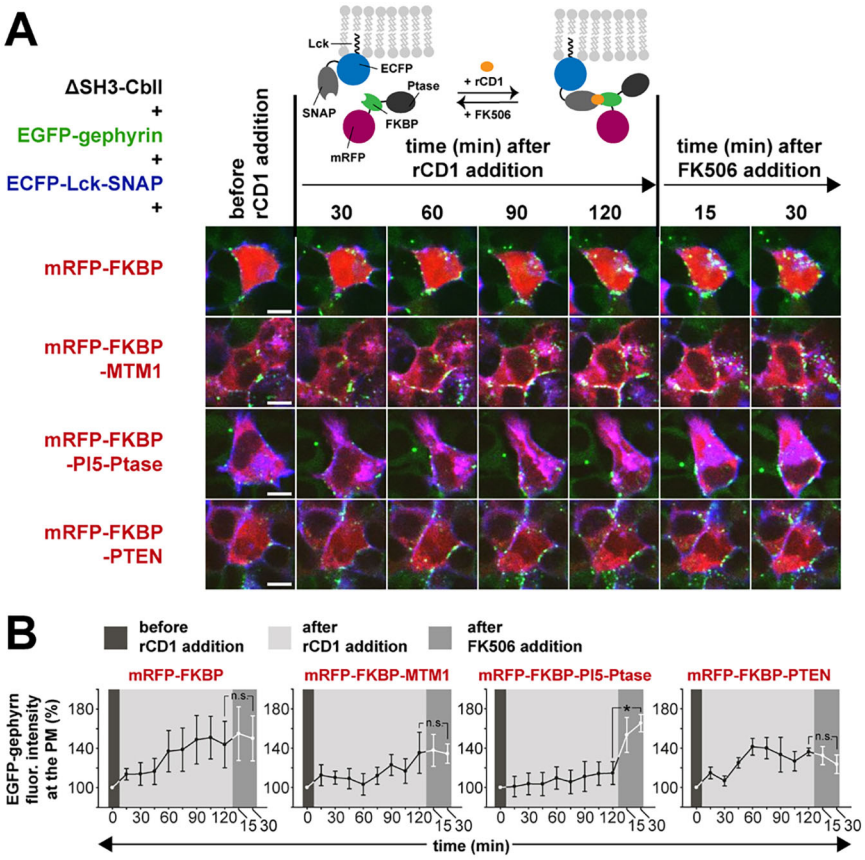

Fig. 6. Plasma membrane PI(4,5)P_2 is required for Cb-dependent formation of gephyrin microclusters. (A) Schematic representation of the rCD1-based dimerization system, and representative time-lapse images of Flp-In T-Rex-EGFP-gephyrin HEK 293 cells. Cells were co-transfected in their non-induced state, as indicated. At 16 h post transfection, EGFP–gephyrin expression was induced by addition of tetracycline (4 µg/ml) for 4 h. Prior to confocal microscopy, the medium was replaced by imaging medium. At the time point indicated, rCD1 (1 µM) was added to induce translocation of the different mRFP–FKBP constructs to the plasma membrane, and each position was imaged every 15 min (for simplicity, only selected time points are shown). FK506 (1 µM) was added at the time point indicated to achieve rapid release of the mRFP-FKBP constructs, as previously shown (Feng et al., 2014). Scale bars: 10 µm. (B) Quantifications of the of EGFP–gephyrin intensity seen at the plasma membrane as a percentage relative to the corresponding intensities at time point 0, as indicated). The corrected total cell fluorescence was calculated as described in the Materials and Methods. The following ratios were calculated: percentage of EGFP–gephyrin fluorescence intensity at time point 30 min after FK506-addition/percentage of EGFP–gephyrin fluorescence intensity at time point 120 min after rCD1 addition (ratios are mRFP–FKBP, 1.055±0.028; mRFP–FKBP–MTM1, 1.067±0.142; mRFP–FKBP–PI5-Ptase, 1.491±0.139; and mRFP–FKBP–PTEN, 0.91±0.076). Data represent means±s.e.m. of *n*=5 cells per condition.

proteins (red), as indicated (Fig. 6A), a TET-induced induction of EGFP–gephyrin (green, Fig. 6A; for images of single EGFP–gephyrin channels, see also Fig. S6) for 4 h allowed for the identification of cells with EGFP–gephyrin submembraneous microclusters induced by ΔSH3-CbII, as shown previously [Papadopoulos et al., 2017; Fig. 6A and Fig. S6, images before rCD1 addition (time point 0 min)]. Time-lapse fluorescence imaging after the addition of 1 µM rCD1 (Fig. 6A; Fig. S6) and quantifications of the EGFP–gephyrin fluorescence at the plasma membrane relative to the corresponding intensities at time point 0 (Fig. 6B) were performed, as shown. This indicated an ∼40%, ∼35% and ∼36% increase in the fluorescence intensities of EGFP–gephyrin between time point 0 min (before rCD1 addition) and time point 120 min after rCD1 addition for mRFP–FKBP, mRFP–FKBP–MTM1 and mRFP–FKBP–PTEN coexpressing cells, respectively (Fig. 6B). This increase in EGFP–gephyrin fluorescence intensity is mostly due to the plasma membrane enrichment of newly expressed EGFP–gephyrin during the time-lapse imaging experiment. In contrast, in cells coexpressing mRFP–FKBP–PI5-Ptase, only a 15% increase in EGFP–gephyrin fluorescence intensity at the plasma membrane between time points 0 min and 120 min after rCD1 addition was observed (Fig. 6B). This result indicates that the translocation of newly synthesized EGFP–gephyrin to the plasma membrane is retarded upon compartment-specific depletion of PI(4,5)P_2 by its cognate phosphatase PI5-Ptase. In order to determine whether the translocation of mRFP–FKBP–PI5-Ptase to the plasma membrane leads to PI(4,5)P_2 depletion, we coexpressed the PH domain of PLCδ1, a specific probe for PI(4,5)P_2, fused to EGFP (EGFP–$PH_{PLC\delta1}$) together with ECFP–Lck–SNAP and mRFP–FKBP–PI5-Ptase in HEK 293 cells (Fig. S7). In the absence of rCD1 (Fig. S7, left), EGFP–$PH_{PLC\delta1}$ mostly localized at the plasma membrane (indicated by arrows in Fig. S7) due to the accumulation of PI(4,5)P_2 at that compartment. Application of 1 µM rCD1 for 2 h led to the depletion of the EGFP–$PH_{PLC\delta1}$ signal from the plasma membrane and to its even redistribution in the cytoplasm and nucleus (Fig. S7, right). This indicates that the rCD1-dependent redistribution of mRFP–FKBP–PI5-Ptase to the plasma membrane leads to compartment-specific degradation of PI(4,5)P_2.

It has been previously shown that upon addition of the competing ligand FK506, rapid release of the mRFP–FKBP fusion proteins from the plasma membrane could be achieved (Feng et al., 2014). In our applications, this permitted us to study not only the effects of depleting a specific phosphoinositide, but also the effects of its subsequent compartment-specific *de novo* biosynthesis in single cells by fluorescence microscopy. Again, release of mRFP–FKBP, mRFP–FKBP–MTM1 or mRFP-FKBP-PTEN from the plasma membrane by addition of 1 µM FK506 to the imaging medium had no apparent effect on the fluorescence intensity of EGFP–gephyrin at the plasma membrane (Fig. 6A,B; Fig. S6). The ratios of the EGFP–gephyrin fluorescence intensity at time point 30 min after FK506 addition to those of EGFP–gephyrin fluorescence intensity at time point 120 min after rCD1 addition (Fig. 6B) were similar between cells expressing mRFP–FKBP–MTM1 and mRFP–FKBP–PTEN (ratios mRFP–FKBP–MTM1, 1.067±0.142; mRFP–FKBP–PTEN, 0.91±0.076; mean±s.e.m.) and not significantly different from that of cells expressing the control construct mRFP–FKBP (ratio 1.055±0.028). In contrast, the corresponding ratio in cells expressing mRFP–FKBP–PI5-Ptase (ratio 1.491±0.139) was significantly increased, as compared to those expressing mRFP–FKBP (Fig. 6B). This result indicates that the translocation of newly synthesized EGFP–gephyrin to the plasma membrane is facilitated

Journal of Cell Science (2020) 133, jcs232835. doi:10.1242/jcs.232835

upon the FK506-mediated release of PI5-Ptase and the subsequent *de novo* biosynthesis of PI(4,5)P_2.

DISCUSSION

In the present study, we provide evidence for a regulatory molecular principle in the formation of GABAergic synapses, where the phosphoinositide preference of Cb is regulated by an interaction with its cognate substrate TC10. This interaction can switch phospholipid ligands from endosome-based to plasma-membrane-based phosphoinositides, thereby promoting the recruitment of gephyrin and $GABA_A$Rs to nascent synapses. Our findings explain the hitherto enigmatic facts that native Cb is present in both endosomal and plasma membrane compartments and that Cb can operate at postsynaptic membranes to recruit gephyrin despite its intrinsic preference for endosome-based phosphoinositides (Fig. 7).

Regulation of TC10 by prenylation and lipid binding

Our analysis of TC10 function in Cb-dependent gephyrin clustering was focused on the hypervariable C-terminal region of TC10. To this end, we generated a series of mutations in TC10 that perturb diverse types of subcellular localization signals. The functionality and characteristics of these TC10 variants were then tested in a well-established cell-based assay that reliably reads out gephyrin redistribution into submembraneous microclusters upon activation of SH3-domain-containing Cb variants by TC10 (Mayer et al., 2013; Papadopoulos et al., 2015; Soykan et al., 2014).

Based on analyses of specific mutants, we found that membrane attachment of TC10 mediated by its prenylation and its C-terminal polybasic stretch is essential for TC10-triggered Cb-dependent clustering of gephyrin at the plasma membrane (Fig. 1B). In contrast, palmitoylation of TC10 is dispensable for this process. In agreement with this result, previous studies showed that the treatment of diverse GFP–TC10-expressing cell types with the palmitoylation inhibitor 2-bromopalmitate (Veit et al., 2001) did not affect the localization of TC10 at the plasma membrane and at endomembranes, indicating that loss of palmitoylation does not cause mislocalization of TC10 (Roberts et al., 2008; Valero et al., 2010).

The importance of phosphoinositides in targeting proteins with polybasic clusters to membranes has been stressed previously (Di Paolo and De Camilli, 2006; Heo et al., 2006). To dissect the role of the polybasic stretch in the TC10 C-terminus, we examined interactions with seven major phosphoinositides using bacterially expressed and purified WT TC10 and a TC10 KR/GS mutant, in which the polybasic stretch is eliminated. Protein-lipid overlay assays indicated specific interactions of TC10 with monophosphorylated phosphoinositides, particularly PI3P and PI5P. Furthermore, SPR analyses indicated enhanced binding of TC10 to PI3P, PI5P and PI(4,5)P_2. All of these interactions were strongly impaired in the TC10 KR/GS mutant. PI3P is the defining phosphoinositide at early/sorting endosomes (Di Paolo and De Camilli, 2006). Accordingly, colocalization analyses using NIH-3T3 cells expressing mCherry–Rab5 together with HA–TC10 WT or the HA–TC10 KR/GS mutant indicated an enrichment of WT TC10 in Rab5-positive endosomes, which was significantly reduced in the case of the HA–TC10 KR/GS mutant. Together, these results show that PI3P binding to the polybasic stretch in the TC10 C-terminus is required for the localization of TC10 on early/sorting endosomes.

This endosomal localization of TC10 may have important implications regarding the mechanisms by which TC10–Cb binding accelerates membrane anchoring of the PH domain of Cb and subsequent clustering of gephyrin at newly formed postsynapses. In line with the notion of a role of TC10 in tuning Cb-dependent inhibitory synapse formation, overexpression of TC10 in cultured hippocampal neurons increases the density and size of gephyrin clusters, particularly at perisomatic synapses (Mayer et al., 2013). Indeed, we found that at nascent perisomatic synapses of DIV 9 neurons that HA–TC10 WT induces a similar stimulatory effect on gephyrin clustering to that we observed previously (Mayer et al., 2013; Fig. 2). In contrast, the HA–TC10 KR/GS mutant showed no such effect, indicating that phosphoinositide-dependent membrane anchoring of TC10 – in addition to its prenylation – is essential for the PH domain of Cb to stabilize a conformation and/or orientation that allows efficient membrane anchoring of Cb and, subsequently, enhances gephyrin clustering at perisomatic synapses. The reason why TC10 overexpression exclusively enhances gephyrin clustering at perisomatic sites is currently unknown, but might reflect the involvement of additional postsynaptic proteins in the Cb-dependent formation of inhibitory synapses. In line with this interpretation, previous studies have indicated that genetic deletion of NL2 in mice leads to a selective loss of gephyrin and $GABA_A$Rs only at

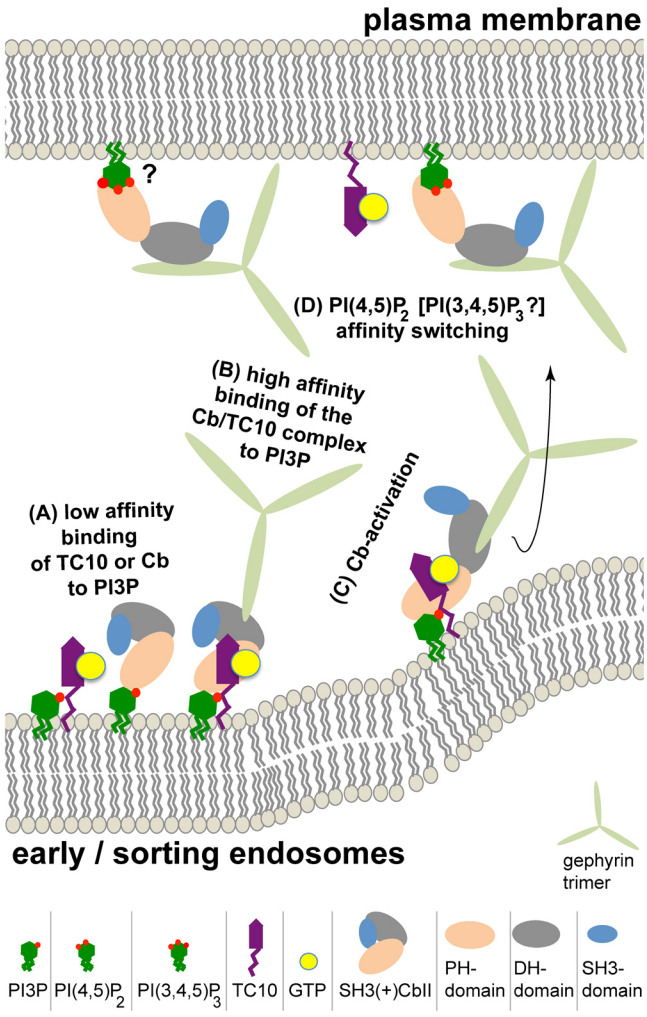

Fig. 7. Tentative model for the role of TC10 in Cb-dependent assembly of the gephyrin scaffold at the plasma membrane. For details, see text in Discussion. There is an initial low affinity interaction between TC10 and PI3P (A), which act cooperatively to recruit Cb at early/sorting endosomes (B). Activation of Cb occurs due prolonged interaction of TC10 with Cb on early/sorting endosomes (C). Active Cb interacts with phosphoinositides enriched at the plasma membrane and recruits gephyrin to nascent inhibitory postsynapses (D).

Journal of Cell Science (2020) 133, jcs232835. doi:10.1242/jcs.232835

perisomatic GABAergic synapses, leaving dendritic GABAergic synapses unaffected (Poulopoulos et al., 2009; Soykan et al., 2014).

The results described above support a model (Fig. 7) according to which the weak interaction of TC10 with PI3P on early/sorting endosomes (Fig. 7A) provides a second membrane anchor for Cb, in addition to the weak Cb–PI3P interaction. The PI3P–TC10 interaction with gephyrin-bound Cb then allows the local enrichment of TC10–Cb–gephyrin complexes at endomembranes (Fig. 7B). In line with this notion, the interaction of TC10–Cb complexes with PI3P in protein-lipid overlay and SPR assays was stronger than the corresponding PI3P interactions of the individual proteins (Fig. 3B, Table 1). Thus, PI3P and TC10 at early/sorting endosomes might act cooperatively to recruit Cb, thereby enriching TC10–Cb–gephyrin complexes on PI3P-rich early/sorting endosomes. This scenario would represent a process of coincidence detection, as previously suggested (Di Paolo and De Camilli, 2006), where coincident signals are amplified by a cooperative action of two different ligands at two different binding sites (Prehoda et al., 2000). In support of this idea, gephyrin can be detected at PI3P-rich endomembranes (Papadopoulos et al., 2017), and a pool of PI3P that is generated by the class III phosphoinositide 3-kinase on early/sorting endosomes plays an important role in clustering gephyrin and $GABA_A$Rs at nascent inhibitory postsynapses (Papadopoulos et al., 2017).

A TC10-induced switch in the phosphoinositide preference of Cb

We proposed previously (Mayer et al., 2013) that the prolonged interaction of TC10 with Cb induces a stronger activation of Cb (Fig. 7C) due to the elimination of intramolecular interactions between the SH3 domain and the DH-PH domain tandem. In analogy to this notion, a recent study indicated that the membrane remodelling activity of sorting nexin 9 (SNX9) is controlled by an allosteric structural switch involving coincidence detection of the clathrin adaptor AP2 and $PI(3,4)P_2$ (Lo et al., 2017). The functional implications of the flexibility in the orientation of the PH domain relative to the DH domain of Cb have been extensively studied previously (Papadopoulos et al., 2015; Soykan et al., 2014). The corresponding studies showed that single mutations affecting either intramolecular interactions between the SH3 domain and the DH-PH tandem domain (Ludolphs et al., 2016; Soykan et al., 2014) or the strength of interactions between the DH and PH domains (Long et al., 2015; Papadopoulos et al., 2015) lead to significant changes in phosphoinositide binding specificity. In essence, these data provided the first indications that conformational changes in Cb can affect its phospholipid preference.

In agreement with this notion, the present study shows that binding of TC10 also affects the phospholipid specificity of Cb. This is indicated by our protein-lipid overlay and SPR assays (Figs 3 and 5 and Table 1). Here, TC10 induces a phospholipid affinity switch on Cb, which allows the protein to specifically interact with additional phosphoinositides that are enriched at the plasma membrane, such as $PI(4,5)P_2$ and $PI(3,4,5)P_3$ (Fig. 7D). Taking into consideration that the TC10 KR/GS mutant is defective in phosphoinositide binding, the strong increase in the interactions of the TC10 KR/GS+GST–SH3(+)CbII mixture with PI3P, $PI(4,5)P_2$ and to a lesser extent with $PI(3,4,5)P_3$, as compared to those in the absence of TC10 KR/GS (Table 1) can be only explained by a conformational switch on the PH domain of Cb. However, whether TC10 remains bound to plasma-membrane-anchored Cb, or dissociates upon the conformational change of the PH domain – which allows stronger interactions with $PI(4,5)P_2$ and $PI(3,4,5)P_3$ – remains to be further investigated. Our model is further supported by our cell biological data obtained with a reversible chemical dimerizer (rCD1; Feng et al., 2014) and time-lapse confocal imaging. These experiments show that elimination of $PI(4,5)P_2$, but not of PI3P or $PI(3,4,5)P_3$, from the plasma membrane of Flp-In T-Rex-EGFP-gephyrin HEK 293 cells overexpressing the constitutively active ΔSH3-CbII isoform attenuates the recruitment of newly synthesized EGFP–gephyrin. In contrast, *de novo* biosynthesis of $PI(4,5)P_2$, due to the release of PI5-Ptase from the plasma membrane upon addition FK506 to the medium, rapidly and significantly increased the EGFP–gephyrin signal in the same compartment. However, we cannot rule out an additional involvement of $PI(3,4,5)P_3$ in the clustering of gephyrin, since phosphoinositide interconversion through PTEN, the 3-phosphatase with the highest preference for $PI(3,4,5)P_3$ (Balla, 2013) used in this study, also increases the level of $PI(4,5)P_2$ at the plasma membrane. Here, additional work will be required to clarify whether both $PI(4,5)P_2$ and $PI(3,4,5)P_3$ are equally involved in the clustering of gephyrin at the plasma membrane.

Conclusion

Based on our data, we propose that TC10 contributes to the formation of inhibitory synapses by regulating at least two consecutive steps during the development of inhibitory postsynapses. First, by enhancing the recruitment of Cb or Cb–gephyrin complexes to PI3P-rich early/sorting endosomes, and second, by inducing a phosphoinositide affinity switch in Cb, which allows stronger interactions with phosphoinositides located at the plasma membrane, thereby leading to efficient translocation of gephyrin to nascent postsynapses. In neurons, the stabilization and maintenance of the postsynaptic scaffold may be further supported by the direct interaction of gephyrin with NL2, NL4 and $GABA_A$Rs (Krueger-Burg et al., 2017).

MATERIALS AND METHODS

cDNA constructs

The pEGFP-C2-gephyrin plasmid (Fuhrmann et al., 2002), the Myc-tagged ΔSH3-CbII and SH3(+)CbII (Harvey et al., 2004; Poulopoulos et al., 2009), the GST-tagged ΔSH3-CbII and SH3(+)CbII (Papadopoulos et al., 2015) constructs have been described previously. The N-terminally HA-tagged TC10 WT, TC10 H-Ras and TC10 K-Ras constructs were a generous gift from Jeffrey E. Pessin (Albert Einstein College of Medicine, Bronx, NY). The GST–TC10 construct was generated by cloning TC10 cDNA into the *Bam*HI/*Eco*RI sites of the pGEX-4T-1 vector (GE Healthcare). The HA-tagged TC10 C210S, C206S, C209S, CC206/9SS, KR/AA, KR/GS and the GST–TC10 KR/GS constructs were generated by oligonucleotide-directed mutagenesis using the QuikChange mutagenesis kit (Stratagene) according to the manufacturer's instructions. The sequences of all mutagenized cDNAs were confirmed by automated DNA sequencing. The mCherry-tagged Rab5 (Rab5a) construct was a generous gift from Jens Rettig (Department of Cellular Neurophysiology, Saarland University, Homburg, Germany). The ECFP–Lck–SNAP, mRFP–FKBP and mRFP–FKBP–PI5-Ptase constructs were a generous gift from Carsten Schultz (Department of Physiology and Pharmacology, Oregon Health and Science University, Portland, OR). The mRFP–FKBP–MTM1 and mRFP–FKBP–PTEN constructs were a generous gift from Volker Haucke (FMP and Freie Universität Berlin, Germany). The EGFP–$PH_{PLC\delta1}$ construct was a generous gift from Mikael Simons (German Center for Neurodegenerative diseases, Munich, Germany).

Antibodies

The following primary antibodies were used for immunocytochemistry: monoclonal mouse anti-gephyrin (mAb7a, cat. no. 147011, Synaptic Systems, 1:1000), polyclonal guinea pig anti-vesicular inhibitory amino acid transporter (VIAAT) (cat. no. 131004, Synaptic Systems, 1:2000),

Journal of Cell Science (2020) 133, jcs232835. doi:10.1242/jcs.232835

polyclonal anti-hemagglutinin (HA) (cat. no. NB600-363, Novus Biologicals, 1:2000) and monoclonal mouse anti-c-Myc clone 9E10 (cat. no. M5546, Sigma-Aldrich, 1:1000). The following secondary antibodies were used for immunocytochemistry: Alexa Fluor 488, 555 or 633-conjugated goat anti-mouse, goat anti-rabbit or goat anti-guinea pig IgGs (Invitrogen, 1:2000). The following antibodies were used for immunoblotting and protein-lipid overlay assays: polyclonal rabbit anti-TC10 (cat. no. ab107573, Abcam, 1:1000) and anti-GST–HRP conjugate (cat. no. RPN1236V, GE Healthcare, 1:10,000). The following secondary antibody was used for immunoblotting and protein-lipid overlay assays: peroxidase-conjugated AffiniPure goat anti-rabbit IgG (Jackson ImmunoResearch Laboratories, 1:10,000).

Purification of TC10- and GST-tagged Cb

GST–SH3(+)CbII and GST–ΔSH3-CbII were bacterially expressed and purified, as described previously (Mayer et al., 2013). GST–TC10 was expressed from pGEX-4T-1 plasmid in the *Rosetta*2 *E. coli* strain. On the day of protein induction, a 1 l lysogeny broth (LB)-ampicillin culture was inoculated with a 50 ml culture grown over night. Bacteria were cultured at 37°C and 250 rpm to an optical density at 600 nm (OD_{600}) of 0.8. The culture was cooled down to 16°C and protein expression was induced with 0.5 mM IPTG overnight at 16°C. Cells were harvested by centrifugation (4550 ***g***, 20 min, 4°C) and resuspended in ice-cold PBS-containing lysozyme (2 mg/ml), DNase I (50–100 µg/ml), 1 mM $MgCl_2$, protease inhibitors (1 µM leupeptin, 1 µg/ml aprotinin and 100 µM PMSF) and 10 mM EDTA. Cells were incubated at 4°C for 10 min and lysed by sonication (VS-70, Sonoplus, Bandelin, two times for 1 min at 100% intensity, 40% cycle). The lysate was cleared by centrifugation at 10,000 ***g*** for 30 min at 4°C. The supernatant was collected and cleared by ultracentrifugation (148,000 ***g***, 30 min, 4°C; Beckmann L-70 ultracentrifuge, rotor type: 50.2 Ti). During this time, glutathione–Sepharose 4B beads (600 µl) were washed three times with 2 ml ice-cold PBS, added to the supernatant upon ultracentrifugation and incubated by rotating for 4 h at 4°C. After washing the beads three times with 20 mM Tris-HCl pH 7.5, 400 mM NaCl, 0.5% (v/v) Triton-X-100, and two times with 20 mM Tris-HCl pH 7.5, 150 mM NaCl, 2 mM EDTA, 1 mM DTT, 10% glycerol (v/v), the beads were resuspended in 900 µl 20 mM Tris-HCl pH 7.5, 150 mM NaCl, 2 mM EDTA, 1 mM DTT, 10% (v/v) glycerol. In order to remove the GST tag from the purified protein, 4 µl thrombin enzyme (Novagen, Thrombin, restriction grade 69671-3) and 100 µl thrombin/cleavage/capture buffer (Novagen-kit 69671-3) were added to the suspension and the beads were incubated at 4°C for 16 h under permanent rotation. Upon centrifugation at 2500 ***g*** for 2 min, the supernatant was collected and an additional centrifugation step at 12,300 ***g*** for 2 min was performed. Finally, 50 µl aliquots of the supernatant were shock-frozen in liquid nitrogen and stored at −80°C. The purity of the untagged TC10 and the successful removal of the GST-tag were confirmed by SDS-PAGE and western blotting using both TC10- and GST-specific antibodies.

In vitro binding assays

For *in vitro* binding assays, TC10 WT or the KR/GS mutant were loaded with GTPγS (Millipore) at 120 µM in 50 mM Tris-HCl (pH 7.5), 1 mM DTT, 5 mM EDTA and protease inhibitors for 20 min at 30°C as described previously (Mayer et al., 2013). The *in vitro* binding assays were performed as described previously (Papadopoulos et al., 2015).

Protein-lipid overlay assays

For protein-lipid overlay assays, TC10 WT or the KR/GS mutant were loaded with GDP or GTPγS (Millipore) at 120 µM in 20 mM Tris-HCl (pH 7.5), 1 mM DTT, 5 mM EDTA and protease inhibitors for 20 min at 30°C as described previously (Mayer et al., 2013). To test relative phosphoinositide-binding affinities of the GTPγS-TC10 KR/GS mutant as compared with GTPγS-TC10 WT in the absence or presence of GST–SH3(+)CbII, or that of GST–ΔSH3-CbII or GST–SH3(+)CbII in the absence or presence of GTPγS-TC10 (WT or the KR/GS mutant) the experiments were carried out as follows. First, custom-made phosphoinositide strips were prepared by spotting 200 pmol of PI3P-, PI4P-, PI5P-, PI(3,4)P_2-, PI(3,5)P_2-, PI(4,5)P_2- and PI(3,4,5)P_3-diC16 (Echelon Biosciences) onto Hybond-C-extra membranes (GE Healthcare). Membranes were then blocked with 3% (w/v) fatty acid-free bovine serum albumin (BSA; A7030, Sigma-Aldrich) in Tris-buffered saline (TBS) pH 7.5. TC10 WT or the KR/GS mutant were preincubated in GTPγS-loading buffer (120 µM GTPγS in 20 mM Tris-HCl pH 7.5, 1 mM DTT and 5 mM EDTA), as described above, and the loading reaction was stopped by adding 10 mM $MgCl_2$. Aliquots of purified GST–ΔSH3-CbII or GST–SH3(+)CbII in 20 mM Tris-HCl, pH, 7.5, 150 mM NaCl, 2 mM EDTA, 1 mM DTT, 10% (v/v) glycerol were diluted 1:1 with either GTPγS-loading buffer (see above) containing 10 mM $MgCl_2$ or with preloaded TC10 (WT or the KR/GS mutant) in GTPγS-loading buffer with 10 mM $MgCl_2$. Subsequently, the Hybond-C-extra membranes spotted with the different phosphoinositides were incubated with 0.5 µg/ml of each protein in TBST [0.1% (v/v) Tween 20 in TBS] with 3% (w/v) BSA for 2 h at room temperature. After four washes with TBST and two washes with TBS, bound proteins were detected with standard dot-blot techniques using a polyclonal rabbit anti-TC10 (ab107573, Abcam, 1:1000) or an anti-GST–HRP conjugate (RPN1236V, GE Healthcare, 1:10,000).

Liposome preparation and SPR analysis of lipid–protein interactions

l-α-phosphatidylcholine (PC) and l-α-phosphatidylethanolamine (PE) were purchased from Avanti Polar Lipids Inc. Phosphoinositides [PI3P; PI4P; PI5P; PI(4,5)P_2 and PI(3,4,5)P_3] were purchased from Echelon Biosciences. Lipids were dissolved in either chloroform to a final concentration of 25 mg/ml (PC and PE) or in a mixture of chloroform, methanol and water (phosphoinositides). Liposomes were prepared as described previously (Tarasenko et al., 2017), by mixing PC and PE in a 70:30 ratio (control liposomes), or PC, PE and the indicated phosphoinositide in a 60:30:10 ratio. Lipid suspensions were dried under continuous nitrogen flow and subsequently desiccated for at least 3 h (to remove water traces). To ensure an appropriate rate of phosphoinositide incorporation into the lipid bilayer, suspensions were supplemented with 2 µl of 1 M HCl. Dried lipids were hydrated in SPR running buffer (20 mM HEPES pH 7.4, 120 mM NaCl, 5 mM KCl) with a final concentration of 5 mg/ml. Large unilammellar vesicles (LUVs) were obtained by repeated freeze-thaw cycles followed by extrusion through a 200 nm diameter membrane (Whatman). The obtained vesicle suspension was diluted (1:100) and further used for SPR interaction experiments.

All lipid-protein interaction experiments were carried out on a Reichert SPR S7500 biosensor. An SPR sensorchip coated with a methyldextran layer containing hydrophobic anchoring molecules was mounted and washed with SPR running buffer (20 mM HEPES pH 7.4, 120 mM NaCl, 5 mM KCl) until a stable baseline was measured. The surface was rinsed of contaminations by injecting 0.1% Triton X-100 solution, followed by several washing steps with SPR running buffer. Subsequently the surface was conditioned with HEPES-buffered saline containing 0.05% SDS. Liposomes containing the indicated phosphoinositides were immobilized on the ligand channel (left) and control liposomes were immobilized on the reference channel (right). Injecting similar concentrations of liposome dilutions yielded comparable responses on either ligand, as well as in the reference channel. For all interaction experiments, a serial dilution of TC10 WT, TC10 KR/GS, GST–SH3(+)CbII, and respective mixtures of TC10 WT with GST–SH3(+)CbII and TC10 KR/GS with GST–SH3(+)CbII [TC10 WT and TC10 KR/GS: 500 nM, 250 nM, 125 nM, 62.5 nM, 31.3 nM, 15.7 nM, 7.9 nM and 4 nM; GST–SH3(+)CbII and mixtures: 125 nM, 62.5 nM, 31.3 nM, 15.7 nM, 7.9 nM, 4 nM, 2 nM and 1 nM], all previously incubated with GTPγS-loading buffer for 10 min at 30°C, followed by addition of 10 mM $MgCl_2$, as described in the 'Protein-lipid overlay assays' section, were injected over the surface and association was followed for 4.5 min, dissociation was then followed for 7 min. The surface was rinsed after each analyte injection by two subsequent injections of 50 mM NaOH, followed by several buffer injections. For each analyte injection, two buffer reference injections were performed.

Transfections and immunostainings

COS7 (CRL-1651) and NIH-3T3 (CRL-1658) cells were purchased from ATCC (LGC Standards GmbH, Germany). Flp-In-T-Rex HEK 293 cells (cat. no. R780-07) were purchased from Invitrogen (Thermo Fisher

Scientific, Germany). All cell lines were tested independently and certified to be free of mycoplasma. Transfections and immunostainings of COS7 cells and NIH-3T3 cells were performed as described previously (Mayer et al., 2013; Papadopoulos et al., 2015). The transfection parameters were optimized in order to achieve low and comparable expression levels of all recombinant proteins analysed. COS7 and NIH-3T3 cells were plated in 24-well plates on 12-mm coverslips and 100 ng of each cDNA were used per well. The empty pcDNA 3.1 vector was used to equalize the total amount of DNA per transfection to 400 ng. Cells were transfected with Lipofectamine 2000 (Invitrogen) following the manufacturer's protocol, fixed 10 h after transfection and stained, as described previously (Mayer et al., 2013). Transfections, treatment and immunostainings of cultured rat hippocampal neurons and Flp-In-T-Rex-EGFP-gephyrin HEK 293 cells were performed as described previously (Papadopoulos et al., 2015, 2017). All animal experiments were performed according to approved guidelines. Images were collected with an inverse Leica DMIRE2 microscope equipped with a 63× oil-immersion objective and connected to a Leica TCS SP2 AOBS confocal laser scanning setup (Leica Microsystems) or with an Axio-Imager Z1 equipped with a Zeiss apochromat 63× objective and an Apotome module (Zeiss).

ImageJ (https://imagej.nih.gov/ij/) was used to analyse immunostainings from images processed under standardized intensity thresholding. For quantifying EGFP–gephyrin fluorescence intensities at the plasma membrane of Flp-In-T-Rex-EGFP-gephyrin HEK 293 cells upon rCD1 or FK506 treatments as a percentage relative to the corresponding intensities at time point 0, the corrected total cell fluorescence (CTCF) was determined. CTCF at the plasma membrane area was calculated by using the ImageJ software package [CTCF=Integrated Density – (Area of selected cell×Mean fluorescence of background readings)].

Time-lapse imaging

For time-lapse imaging, Flp-In-T-Rex-EGFP-gephyrin HEK 293 cells were grown onto poly-L-lysine-coated 15 µ-slide four-well dishes with a glass bottom (cat. no. 80427, Ibidi). EGFP–gephyrin expression was induced 16 h after transfection by adding 4 µg/ml tetracycline (Sigma-Aldrich) to the medium. After 4 h, the cells were washed once and replaced with 250 µl pre-warmed imaging medium (phenol-free DMEM, cat. no. 21063-029, Gibco, Life Technologies). Time-lapse confocal imaging was performed at 37°C and 5% CO_2 using a Nikon Eclipse Ti microscope, equipped with a 40x air objective (0.95NA) and a Yokogawa W1 spinning disk. An Andor iXon 888 camera was used to sequentially acquire multi-channel (mRFP, EGFP and ECFP) *z*-stacks at 5 fields of view per well within the optically compatible four-well Ibidi dishes. The channels were acquired according to the following excitation/emission scenario: (1) 561 nm excitation; 600/52 nm emission (mRFP), (2) 488 nm excitation; 525/50 nm emission (EGFP) and (3) 445 nm excitation; 480/40 nm emission (ECFP). Each position was successively imaged 12 times every 15 min, once before the addition of rCD1, eight times after the addition of rCD1 (1 µM) and three times after the addition of 1 µM FK506 (1 µM). The synthesis and characterization of the reversible chemical dimerizer, rCD1, was described previously (Feng et al., 2014). FK506 was purchased from Tocris Bioscience.

Statistics

Experimental data were evaluated by investigators blind to experimental conditions. Statistical significance was tested by either using the unpaired two-tailed Student's *t*-test or the one-way ANOVA variance test followed by a Tukey multiple comparison test, always applying a 95% confidence interval. The sample sizes (n) were estimated based on previous experiences with similar experiments (Mayer et al., 2013; Papadopoulos et al., 2015). Values represent means±s.e.m. Asterisks indicate significant differences (*P<0.05; **P<0.01; ***P<0.001); n.s. indicates no significant difference. The statistics were evaluated using the GraphPad Prism software.

Acknowledgements

We thank Drs Carsten Schultz, Jeffrey E. Pessin, Volker Haucke, Mikael Simons and Jens Rettig for reagents and plasmids. We are grateful to Dr Nils Brose for valuable scientific advice.

Competing interests

The authors declare no competing or financial interests.

Author contributions

Conceptualization: M.K., S.M., B.S., T.P.; Methodology: M.K., S.M., M.M., H.R., J.H., B.S., T.P.; Software: M.K., S.M., M.M., H.R., T.P.; Validation: M.K., S.M., M.M., H.R., J.H., B.S., T.P.; Formal analysis: M.K., S.M., J.H., T.P.; Investigation: M.K., S.M., T.P.; Resources: M.K., S.M., T.P.; Data curation: M.K., S.M., T.P.; Writing - original draft: M.K., S.M., M.M., B.S., T.P.; Writing - review & editing: M.K., S.M., M.M., H.R., J.H., B.S., T.P.; Visualization: M.K., S.M., T.P.; Supervision: B.S., T.P.; Project administration: B.S., T.P.; Funding acquisition: T.P.

Funding

This work was supported by the Deutsche Forschungsgemeinschaft (grant PA 2087/1-4).

Supplementary information

Supplementary information available online at
http://jcs.biologists.org/lookup/doi/10.1242/jcs.232835.supplemental

References

Balla, T. (2013). Phosphoinositides: tiny lipids with giant impact on cell regulation. *Physiol. Rev.* **93**, 1019-1137. doi:10.1152/physrev.00028.2012

Chiou, T.-T., Bonhomme, B., Jin, H., Miralles, C. P., Xiao, H., Fu, Z., Harvey, R. J., Harvey, K., Vicini, S. and De Blas, A. L. (2011). Differential regulation of the postsynaptic clustering of gamma-aminobutyric acid type A ($GABA_A$) receptors by collybistin isoforms. *J. Biol. Chem.* **286**, 22456-22468. doi:10.1074/jbc.M111.236190

Chiou, T.-T., Long, P., Schumann-Gillett, A., Kanamarlapudi, V., Haas, S. A., Harvey, K., O'Mara, M. L., De Blas, A. L., Kalscheuer, V. M. and Harvey, R. J. (2019). Mutation p.R356Q in the collybistin phosphoinositide binding site is associated with mild intellectual disability. *Front. Mol. Neurosci.* **12**, 60. doi:10.3389/fnmol.2019.00060

Christoforidis, S., Miaczynska, M., Ashman, K., Wilm, M., Zhao, L., Yip, S.-C., Waterfield, M. D., Backer, J. M. and Zerial, M. (1999). Phosphatidylinositol-3-OH kinases are Rab5 effectors. *Nat. Cell Biol.* **1**, 249-252. doi:10.1038/12075

de Groot, C., Floriou-Servou, A., Tsai, Y. C., Fruh, S., Kohler, M., Parkin, G., Schwerdel, C., Bosshard, G., Kaila, K., Fritschy, J. M. et al. (2017). RhoGEF9 splice isoforms influence neuronal maturation and synapse formation downstream of alpha2 $GABA_A$ receptors. *PLoS Genet.* **13**, e1007073. doi:10.1371/journal.pgen.1007073

Di Paolo, G. and De Camilli, P. (2006). Phosphoinositides in cell regulation and membrane dynamics. *Nature* **443**, 651-657. doi:10.1038/nature05185

Feng, G., Steinbach, J. H. and Sanes, J. R. (1998). Rapsyn clusters neuronal acetylcholine receptors but is inessential for formation of an interneuronal cholinergic synapse. *J. Neurosci.* **18**, 4166-4176. doi:10.1523/JNEUROSCI.18-11-04166.1998

Feng, S., Laketa, V., Stein, F., Rutkowska, A., MacNamara, A., Depner, S., Klingmuller, U., Saez-Rodriguez, J. and Schultz, C. (2014). A rapidly reversible chemical dimerizer system to study lipid signaling in living cells. *Angew. Chem. Int. Ed. Engl.* **53**, 6720-6723. doi:10.1002/anie.201402294

Fuhrmann, J. C., Kins, S., Rostaing, P., El Far, O., Kirsch, J., Sheng, M., Triller, A., Betz, H. and Kneussel, M. (2002). Gephyrin interacts with Dynein light chains 1 and 2, components of motor protein complexes. *J. Neurosci.* **22**, 5393-5402. doi:10.1523/JNEUROSCI.22-13-05393.2002

Harvey, K., Duguid, I. C., Alldred, M. J., Beatty, S. E., Ward, H., Keep, N. H., Lingenfelter, S. E., Pearce, B. R., Lundgren, J., Owen, M. J. et al. (2004). The GDP-GTP exchange factor collybistin: an essential determinant of neuronal gephyrin clustering. *J. Neurosci.* **24**, 5816-5826. doi:10.1523/JNEUROSCI.1184-04.2004

Hemsath, L., Dvorsky, R., Fiegen, D., Carlier, M.-F. and Ahmadian, M. R. (2005). An electrostatic steering mechanism of Cdc42 recognition by Wiskott-Aldrich syndrome proteins. *Mol. Cell* **20**, 313-324. doi:10.1016/j.molcel.2005.08.036

Heo, W. D., Inoue, T., Park, W. S., Kim, M. L., Park, B. O., Wandless, T. J. and Meyer, T. (2006). PI(3,4,5)P3 and PI(4,5)P2 lipids target proteins with polybasic clusters to the plasma membrane. *Science* **314**, 1458-1461. doi:10.1126/science.1134389

Hoon, M., Soykan, T., Falkenburger, B., Hammer, M., Patrizi, A., Schmidt, K.-F., Sassoe-Pognetto, M., Lowel, S., Moser, T., Taschenberger, H. et al. (2011). Neuroligin-4 is localized to glycinergic postsynapses and regulates inhibition in the retina. *Proc. Natl. Acad. Sci. USA* **108**, 3053-3058. doi:10.1073/pnas.1006946108

Kalscheuer, V. M., Musante, L., Fang, C., Hoffmann, K., Fuchs, C., Carta, E., Deas, E., Venkateswarlu, K., Menzel, C., Ullmann, R. et al. (2009). A balanced chromosomal translocation disrupting ARHGEF9 is associated with epilepsy, anxiety, aggression, and mental retardation. *Hum. Mutat.* **30**, 61-68. doi:10.1002/humu.20814

Kins, S., Betz, H. and Kirsch, J. (2000). Collybistin, a newly identified brain-specific GEF, induces submembrane clustering of gephyrin. *Nat. Neurosci.* **3**, 22-29. doi:10.1038/71096

Krueger-Burg, D., Papadopoulos, T. and Brose, N. (2017). Organizers of inhibitory synapses come of age. *Curr. Opin. Neurobiol.* **45**, 66-77. doi:10.1016/j.conb.2017.04.003

Liu, M., Bi, F., Zhou, X. and Zheng, Y. (2012). Rho GTPase regulation by miRNAs and covalent modifications. *Trends Cell Biol.* **22**, 365-373. doi:10.1016/j.tcb.2012.04.004

Lo, W.-T., Vujičić Žagar, A., Gerth, F., Lehmann, M., Puchkov, D., Krylova, O., Freund, C., Scapozza, L., Vadas, O. and Haucke, V. (2017). A coincidence detection mechanism controls PX-BAR domain-mediated endocytic membrane remodeling via an allosteric structural switch. *Dev. Cell* **43**, 522-529. doi:10.1016/j.devcel.2017.10.019

Long, P., May, M. M., James, V. M., Granno, S., Johnson, J. P., Tarpey, P., Stevenson, R. E., Harvey, K., Schwartz, C. E. and Harvey, R. J. (2015). Missense mutation R338W in ARHGEF9 in a family with X-linked intellectual disability with variable macrocephaly and macro-orchidism. *Front. Mol. Neurosci.* **8**, 83. doi:10.3389/fnmol.2015.00083

Ludolphs, M., Schneeberger, D., Soykan, T., Schäfer, J., Papadopoulos, T., Brose, N., Schindelin, H. and Steinem, C. (2016). Specificity of collybistin-phosphoinositide interactions: impact of the individual protein domains. *J. Biol. Chem.* **291**, 244-254. doi:10.1074/jbc.M115.673400

Luscher, B., Fuchs, T. and Kilpatrick, C. L. (2011). $GABA_A$ receptor trafficking-mediated plasticity of inhibitory synapses. *Neuron* **70**, 385-409. doi:10.1016/j.neuron.2011.03.024

Mayer, S., Kumar, R., Jaiswal, M., Soykan, T., Ahmadian, M. R., Brose, N., Betz, H., Rhee, J.-S. and Papadopoulos, T. (2013). Collybistin activation by GTP-TC10 enhances postsynaptic gephyrin clustering and hippocampal GABAergic neurotransmission. *Proc. Natl. Acad. Sci. USA* **110**, 20795-20800. doi:10.1073/pnas.1309078110

Michaelson, D., Silletti, J., Murphy, G., D'Eustachio, P., Rush, M. and Philips, M. R. (2001). Differential localization of Rho GTPases in live cells: regulation by hypervariable regions and RhoGDI binding. *J. Cell Biol.* **152**, 111-126. doi:10.1083/jcb.152.1.111

Murphy, G. A., Jillian, S. A., Michaelson, D., Philips, M. R., D'Eustachio, P. and Rush, M. G. (2001). Signaling mediated by the closely related mammalian Rho family GTPases TC10 and Cdc42 suggests distinct functional pathways. *Cell Growth Differ.* **12**, 157-167.

Murray, J. T., Panaretou, C., Stenmark, H., Miaczynska, M. and Backer, J. M. (2002). Role of Rab5 in the recruitment of hVps34/p150 to the early endosome. *Traffic* **3**, 416-427. doi:10.1034/j.1600-0854.2002.30605.x

Neudauer, C. L., Joberty, G., Tatsis, N. and Macara, I. G. (1998). Distinct cellular effects and interactions of the Rho-family GTPase TC10. *Curr. Biol.* **8**, 1151-1161. doi:10.1016/S0960-9822(07)00486-1

Papadopoulos, T., Korte, M., Eulenburg, V., Kubota, H., Retiounskaia, M., Harvey, R. J., Harvey, K., O'Sullivan, G. A., Laube, B., Hülsmann, S. et al. (2007). Impaired GABAergic transmission and altered hippocampal synaptic plasticity in collybistin-deficient mice. *EMBO J.* **26**, 3888-3899. doi:10.1038/sj.emboj.7601819

Papadopoulos, T., Eulenburg, V., Reddy-Alla, S., Mansuy, I. M., Li, Y. and Betz, H. (2008). Collybistin is required for both the formation and maintenance of GABAergic postsynapses in the hippocampus. *Mol. Cell. Neurosci.* **39**, 161-169. doi:10.1016/j.mcn.2008.06.006

Papadopoulos, T., Schemm, R., Grubmüller, H. and Brose, N. (2015). Lipid binding defects and perturbed synaptogenic activity of a collybistin R290H mutant that causes epilepsy and intellectual disability. *J. Biol. Chem.* **290**, 8256-8270. doi:10.1074/jbc.M114.633024

Papadopoulos, T., Rhee, H. J., Subramanian, D., Paraskevopoulou, F., Mueller, R., Schultz, C., Brose, N., Rhee, J.-S. and Betz, H. (2017). Endosomal phosphatidylinositol 3-phosphate promotes gephyrin clustering and GABAergic neurotransmission at inhibitory postsynapses. *J. Biol. Chem.* **292**, 1160-1177. doi:10.1074/jbc.M116.771592

Poulopoulos, A., Aramuni, G., Meyer, G., Soykan, T., Hoon, M., Papadopoulos, T., Zhang, M., Paarmann, I., Fuchs, C., Harvey, K. et al. (2009). Neuroligin 2 drives postsynaptic assembly at perisomatic inhibitory synapses through gephyrin and collybistin. *Neuron* **63**, 628-642. doi:10.1016/j.neuron.2009.08.023

Prehoda, K. E., Scott, J. A., Mullins, R. D. and Lim, W. A. (2000). Integration of multiple signals through cooperative regulation of the N-WASP-Arp2/3 complex. *Science* **290**, 801-806. doi:10.1126/science.290.5492.801

Raiborg, C., Schink, K. O. and Stenmark, H. (2013). Class III phosphatidylinositol 3-kinase and its catalytic product PtdIns3P in regulation of endocytic membrane traffic. *FEBS J.* **280**, 2730-2742. doi:10.1111/febs.12116

Reddy-Alla, S., Schmitt, B., Birkenfeld, J., Eulenburg, V., Dutertre, S., Böhringer, C., Götz, M., Betz, H. and Papadopoulos, T. (2010). PH-domain-driven targeting of collybistin but not Cdc42 activation is required for synaptic gephyrin clustering. *Eur. J. Neurosci.* **31**, 1173-1184. doi:10.1111/j.1460-9568.2010.07149.x

Reid, T., Bathoorn, A., Ahmadian, M. R. and Collard, J. G. (1999). Identification and characterization of hPEM-2, a guanine nucleotide exchange factor specific for Cdc42. *J. Biol. Chem.* **274**, 33587-33593. doi:10.1074/jbc.274.47.33587

Roberts, P. J., Mitin, N., Keller, P. J., Chenette, E. J., Madigan, J. P., Currin, R. O., Cox, A. D., Wilson, O., Kirschmeier, P. and Der, C. J. (2008). Rho Family GTPase modification and dependence on CAAX motif-signaled posttranslational modification. *J. Biol. Chem.* **283**, 25150-25163. doi:10.1074/jbc.M800882200

Roth, M. G. (2004). Phosphoinositides in constitutive membrane traffic. *Physiol. Rev.* **84**, 699-730. doi:10.1152/physrev.00033.2003

Saiepour, L., Fuchs, C., Patrizi, A., Sassoè-Pognetto, M., Harvey, R. J. and Harvey, K. (2010). Complex role of collybistin and gephyrin in $GABA_A$ receptor clustering. *J. Biol. Chem.* **285**, 29623-29631. doi:10.1074/jbc.M110.121368

Schwartz, S. L., Cao, C., Pylypenko, O., Rak, A. and Wandinger-Ness, A. (2007). Rab GTPases at a glance. *J. Cell Sci.* **120**, 3905-3910. doi:10.1242/jcs.015909

Soykan, T., Schneeberger, D., Tria, G., Buechner, C., Bader, N., Svergun, D., Tessmer, I., Poulopoulos, A., Papadopoulos, T., Varoqueaux, F. et al. (2014). A conformational switch in collybistin determines the differentiation of inhibitory postsynapses. *EMBO J.* **33**, 2113-2133. doi:10.15252/embj.201488143

Tanabe, K., Tachibana, T., Yamashita, T., Che, Y. H., Yoneda, Y., Ochi, T., Tohyama, M., Yoshikawa, H. and Kiyama, H. (2000). The small GTP-binding protein TC10 promotes nerve elongation in neuronal cells, and its expression is induced during nerve regeneration in rats. *J. Neurosci.* **20**, 4138-4144. doi:10.1523/JNEUROSCI.20-11-04138.2000

Tarasenko, D., Barbot, M., Jans, D. C., Kroppen, B., Sadowski, B., Heim, G., Möbius, W., Jakobs, S. and Meinecke, M. (2017). The MICOS component Mic60 displays a conserved membrane-bending activity that is necessary for normal cristae morphology. *J. Cell Biol.* **216**, 889-899. doi:10.1083/jcb.201609046

Valero, R. A., Oeste, C. L., Stamatakis, K., Ramos, I., Herrera, M., Boya, P. and Pérez-Sala, D. (2010). Structural determinants allowing endolysosomal sorting and degradation of endosomal GTPases. *Traffic* **11**, 1221-1233. doi:10.1111/j.1600-0854.2010.01091.x

Veit, M., Laage, R., Dietrich, L., Wang, L. and Ungermann, C. (2001). Vac8p release from the SNARE complex and its palmitoylation are coupled and essential for vacuole fusion. *EMBO J.* **20**, 3145-3155. doi:10.1093/emboj/20.12.3145

Vicinanza, M., D'Angelo, G., Di Campli, A. and De Matteis, M. A. (2008). Function and dysfunction of the PI system in membrane trafficking. *EMBO J.* **27**, 2457-2470. doi:10.1038/emboj.2008.169

Watson, R. T., Shigematsu, S., Chiang, S.-H., Mora, S., Kanzaki, M., Macara, I. G., Saltiel, A. R. and Pessin, J. E. (2001). Lipid raft microdomain compartmentalization of TC10 is required for insulin signaling and GLUT4 translocation. *J. Cell Biol.* **154**, 829-840. doi:10.1083/jcb.200102078

Watson, R. T., Furukawa, M., Chiang, S.-H., Boeglin, D., Kanzaki, M., Saltiel, A. R. and Pessin, J. E. (2003). The exocytotic trafficking of TC10 occurs through both classical and nonclassical secretory transport pathways in 3T3L1 adipocytes. *Mol. Cell. Biol.* **23**, 961-974. doi:10.1128/MCB.23.3.961-974.2003

Wenk, M. R. and De Camilli, P. (2004). Protein-lipid interactions and phosphoinositide metabolism in membrane traffic: insights from vesicle recycling in nerve terminals. *Proc. Natl. Acad. Sci. USA* **101**, 8262-8269. doi:10.1073/pnas.0401874101

Winter-Vann, A. M. and Casey, P. J. (2005). Post-prenylation-processing enzymes as new targets in oncogenesis. *Nat. Rev. Cancer* **5**, 405-412. doi:10.1038/nrc1612

FIGURE S1

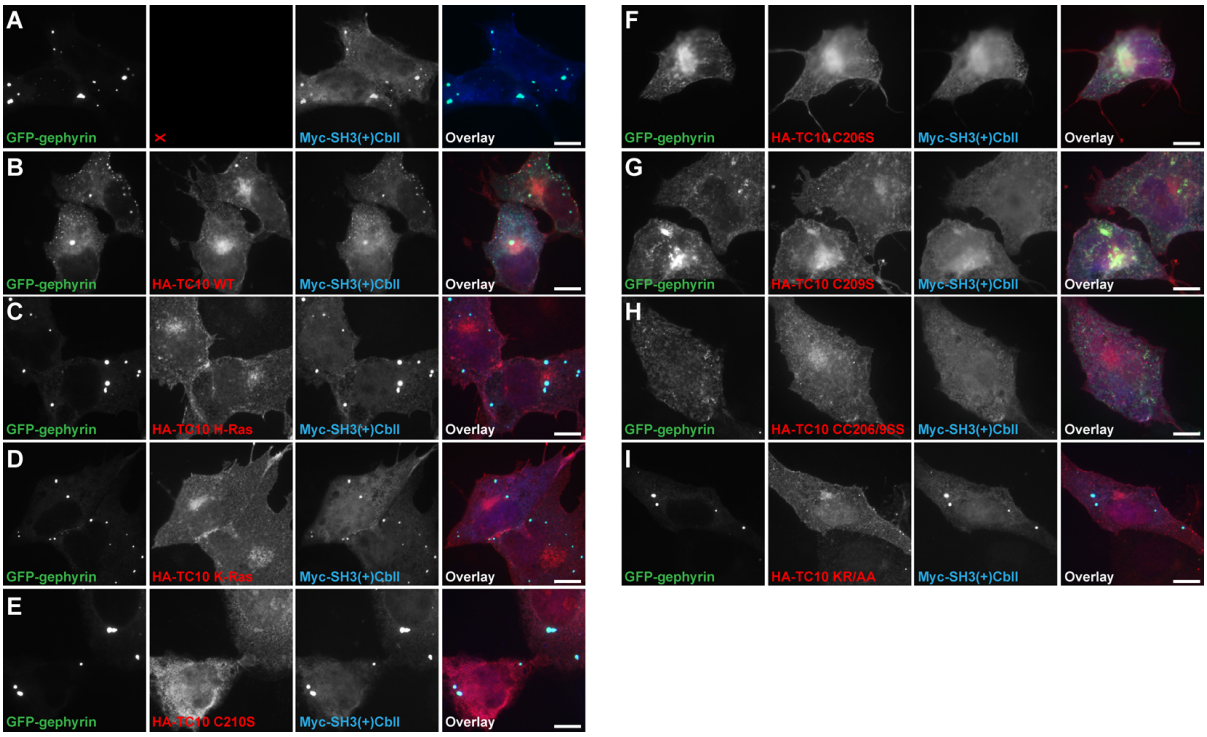

Fig. S1. Effects of the different HA-TC10 mutants on the Cb-mediated clustering of gephyrin in COS7 cells. Representative images of COS7 cells cotransfected with GFP-gephyrin and Myc-SH3(+)CbII in the presence or absence of HA-TC10 WT or mutant proteins, as indicated, and used in the quantifications shown in Fig. 1B. Scale bars: 10 μm.

FIGURE S2

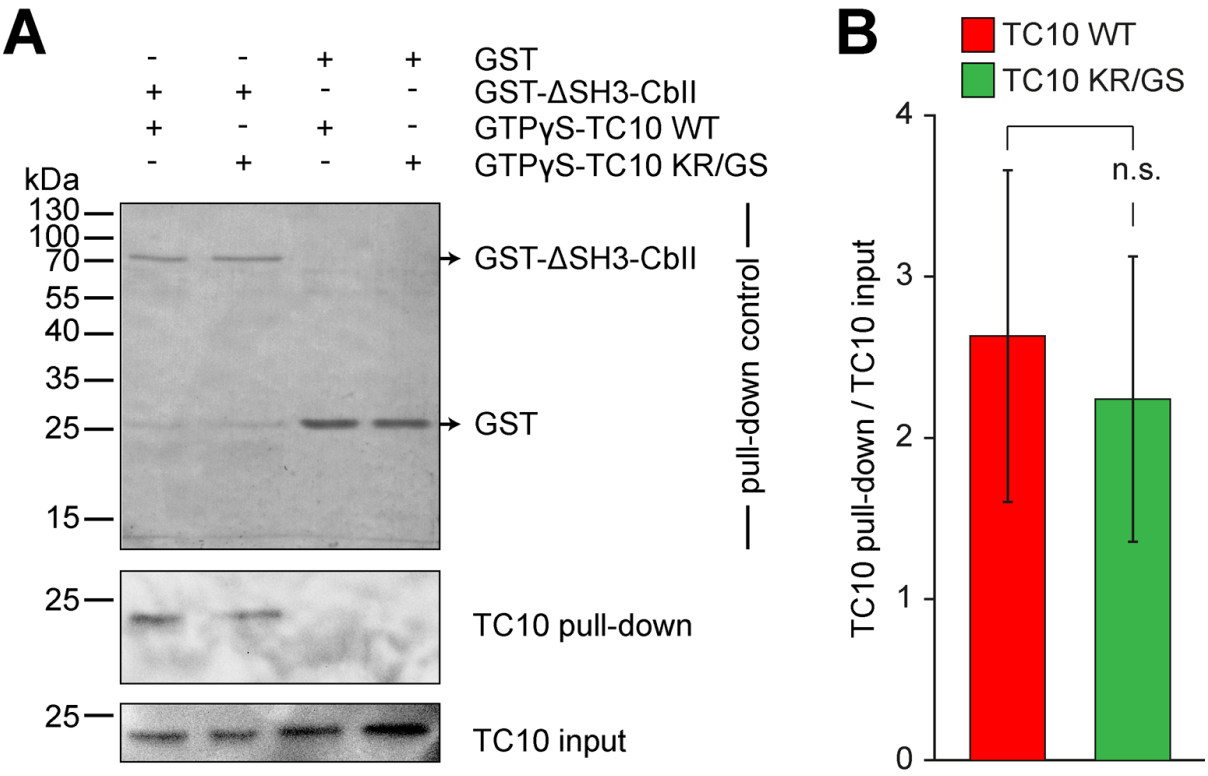

Fig. S2. The TC10 KR/GS mutant retains its binding to Cb. (A) Purified and GTPγS-loaded TC10 WT or the TC10 KR/GS mutant were incubated with the indicated recombinant proteins bound to glutathione-Sepharose beads. Center panel: Bound TC10 (WT or KR/GS) was detected by Western blotting using a TC10-specific polyclonal antibody (TC10 107573, 1:1000; Abcam). Note that both, TC10 WT and the TC10 KR/GS mutant bound to GST-ΔSH3-CbII but not to GST alone. Top pannel: MemCode stainings of the same membrane prior to TC10 immunoblotting indicating the amounts of GST-tagged bait proteins used in the actual reaction mixture. Bottom panel: To ensure that similar amounts of TC10 were included in all reaction mixtures, 2% of the premixed reactions were stored and subsequently subjected to anti-TC10 Western blotting using the TC10 107573 antibody. (B) Quantifications (ratios of relative band intensities of pulled down TC10 / total TC10) of TC10 WT or the KR/GS mutant bound to GST-ΔSH3-CbII. Data represent means ± SEM (n.s., not significant; unpaired, two-tailed Student's t-test) of n=3 independent experiments.

FIGURE S3

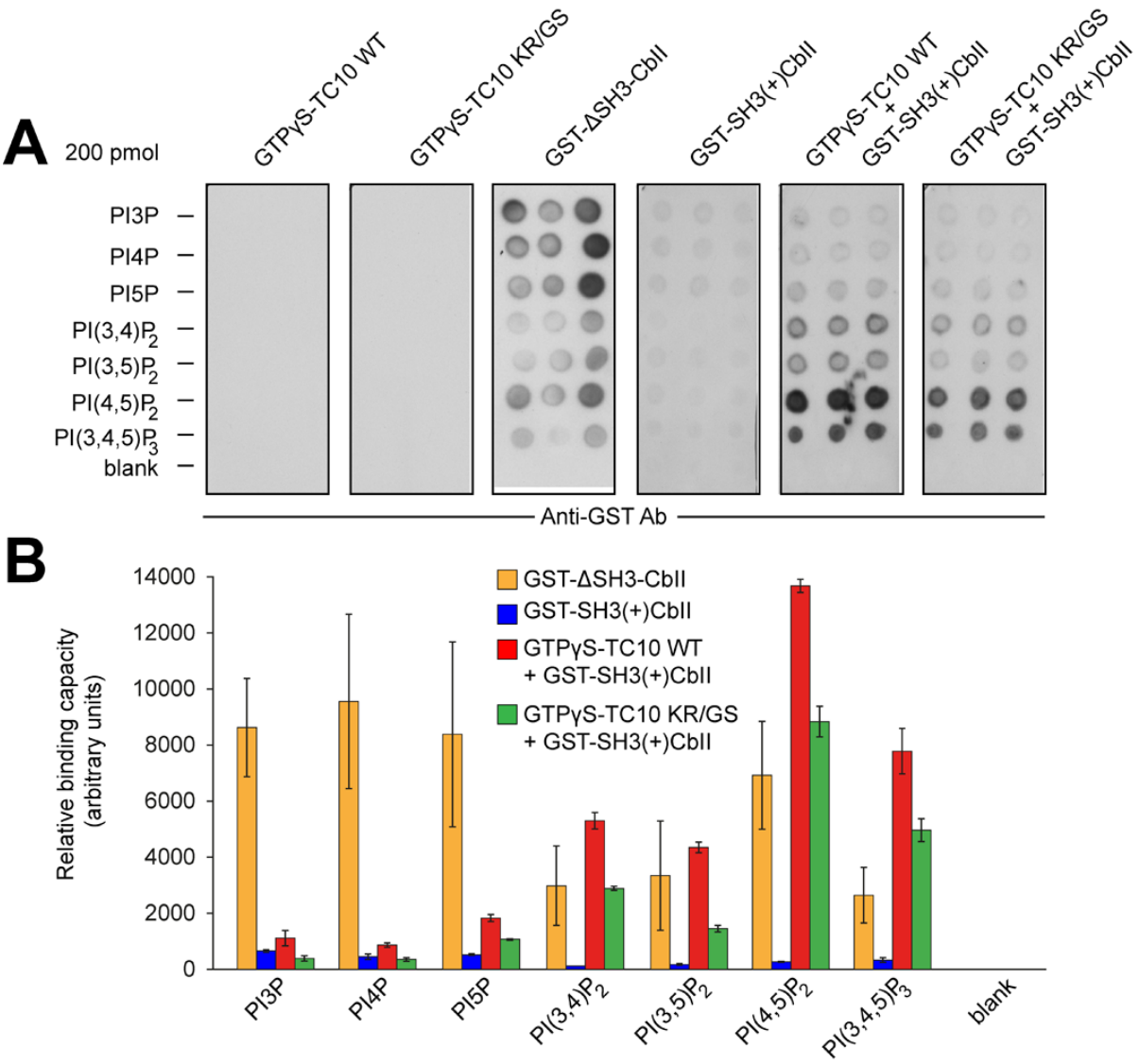

Fig. S3. Both TC10 WT and TC10 KR/GS specifically regulate the binding of Cb to certain phosphoinositides. (A) Protein-lipid overlay assays using GTPγS-TC10 WT, GTPγS-TC10 KR/GS and GST-ΔSH3-CblI, or GST-SH3(+)CblI, either alone or in a 1:1 ratio (0.5 µg/ml of each protein), as indicated on the top of the membranes. 200 pmol of the different phosphoinositides (Echelon, PInPs-diC16) were spotted onto the Hybond-C-extra membranes (GE Healthcare), as indicated. Interactions of Cb with the different phosphoinositides were detected by incubating the membranes with a goat anti-GST-HRP conjugate (GE Healthcare). As shown previously (Ludolphs et al., 2016), ΔSH3-CblI binds to a broad range of phosphoinositides, including monophosphorylated (PI3P, PI4P, PI5P) and diphosphorylated [$PI(4,5)P_2$] ones. However, in contrast to Ludolphs et al., 2016, an elevated interaction of ΔSH3-CblI with $PI(3,4,5)P_3$ was not observed, possibly a consequence of the fact that in

protein lipid overlay assays the phosphoinositides are not embedded in a lipid membrane, and therefore the headgroup posititions of the phosphorylated inositols are neither defined, nor aligned, which may alter binding specificity. In agreement with a previous study (Soykan et al., 2014), the major Cb-isoform in the mammalian brain, SH3-CbII, which forms an autoinhibited conformation in which the SH3 domain interacts with the DH/PH tandem-domain, does not bind to any phosphoinositides. In the presence of both, TC10 (WT or the KR/GS mutant) and Cb, the SH3-CbII isoform shows altered binding capacities for certain phoshoinositides. (B) Relative phosphoinositide binding capacities of proteins, as indicated, determined by measuring the intensity of the chemiluminescence. The data represent means ± SEM of n=3 measurements.

FIGURE S4

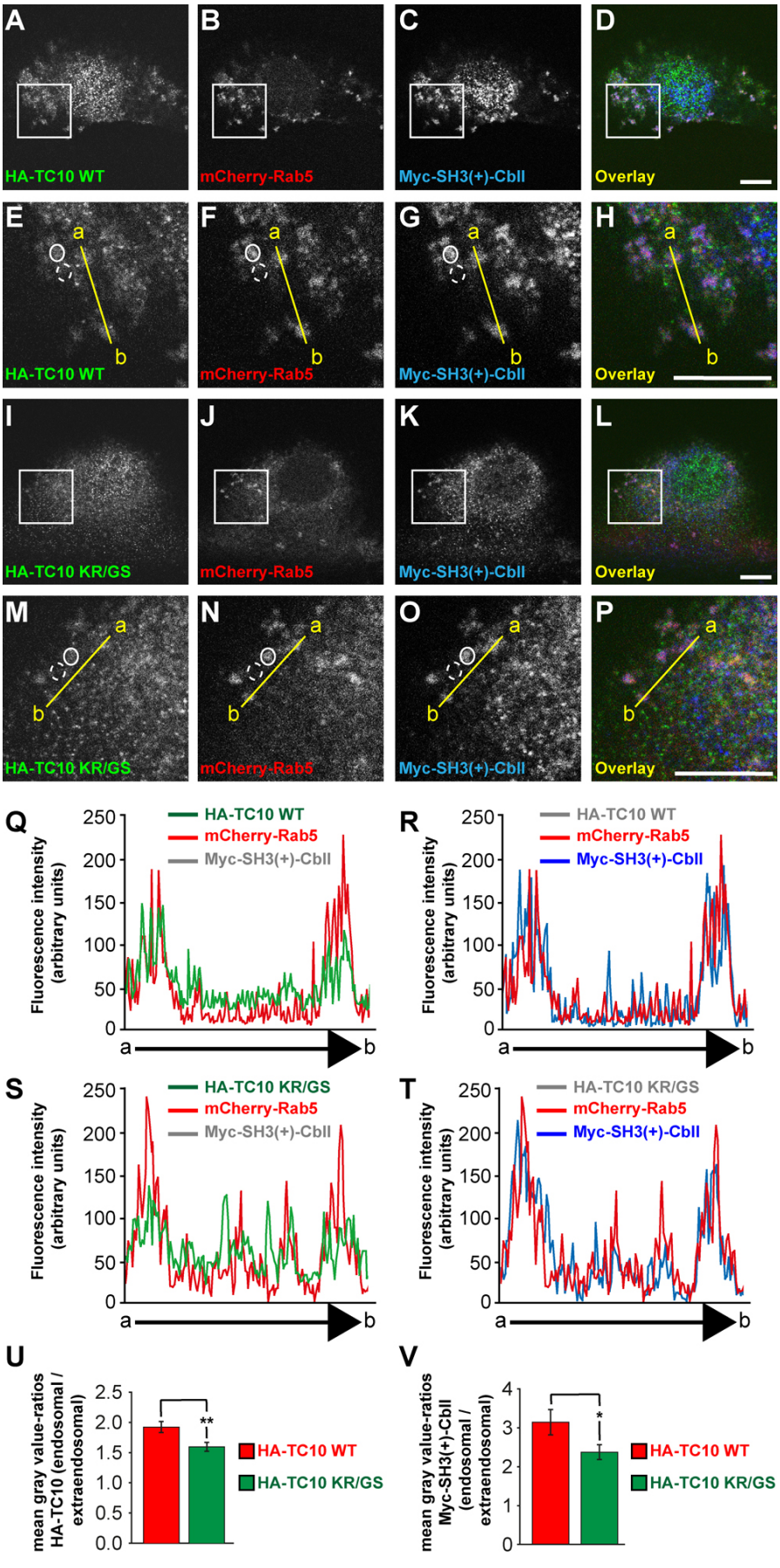

Fig. S4. The KR/GS mutation affects the localization of Myc-SH3(+)-CbII/HA-TC10 complexes at mCherry-Rab5-labeled endosomes.

(A-P) Exemplary confocal images of NIH-3T3 cells coexpressing HA-TC10 WT (A-H) or the HA-TC10 KR/GS mutant (I-P) together with Myc-SH3(+)-CbII and mCherry-Rab5, as indicated. (E-H and M-P) Magnifications of the boxed areas in A-D and I-L, respectively. Note the enriched immunoreactive signal of HA-TC10 WT (E; closed circle) and Myc-SH3(+)CbII (G; closed circle) in mCherry-Rab5-positive endosomes (F; closed circle), as compared to the signal in extraendosomal areas (dashed circles in E-G). In contrast, the endosomal accumulation of both, the HA-TC10 KR/GS mutant (M) and Myc-SH3(+)-CbII (O) was reduced, but not completely diminished in cells coexpressing these two proteins together with mCherry-Rab5 (M-O). Scale bars: 10 µm. (Q, S) Fluorescence intensity scans over the yellow lines in *E-H and M-P* [E: HA-TC10 WT, green; M: HA-TC10 KR/GS, green; F, N: mCherry-Rab5, red; Myc-SH3(+)-CbII in grey indicates that its corresponding fluorescence intensity scan is not shown], respectively. The line plots indicate accumulation of HA-TC10 WT (Q) and strongly reduced accumulation of the HA-TC10 KR/GS mutant (S) in mCherry-Rab5-positive endosomes. (R, T) Fluorescence intensity scans over the yellow lines in *E-H and M-P* [G: Myc-SH3(+)-CbII together with HA-TC10 WT, green; O: Myc-SH3(+)-CbII together with HA-TC10 KR/GS, green; F, N: mCherry-Rab5, red; HA-TC10 (WT or KR/GS) in grey indicates that the corresponding fluorescence intensity scan are not shown], respectively. The line plots indicate clear endosomal accumulation of Myc-SH3(+)-CbII in HA-TC10 WT coexpressing cells (R). The endosomal accumulation of Myc-SH3(+)-CbII in cells coexpressing the HA-TC10 KR/GS mutant is reduced, as compared to the extraendosomal signal in R and T. (U, V) For statistical comparison, the following ratios were calculated: (U) mean gray values of endosomal HA-TC10 / mean gray values of extraendosomal HA-TC10 [WT (red) or the KR/GS mutant (green)] and (V) mean gray values of endosomal Myc-SH3(+)-CbII / mean gray values of extraendosomal Myc-SH3(+)-CbII [in HA-TC10 WT (red) or HA-TC10 KR/GS expressing cells (green)]. Endosomal (closed circles) and extraendosomal (dashed circles) areas were preselected as exemplary indicated by the closed and dashed circles in *E* and *M*, respectively. For each cell, the mean gray values of at least 10 endosomal and 10 extraendosomal areas were calculated. The data represent means ± SEM (*P < 0.05, **P < 0.01; unpaired, two-tailed Student's t-test) of N=3 independent experiments and n=20 cells per condition.

FIGURE S5

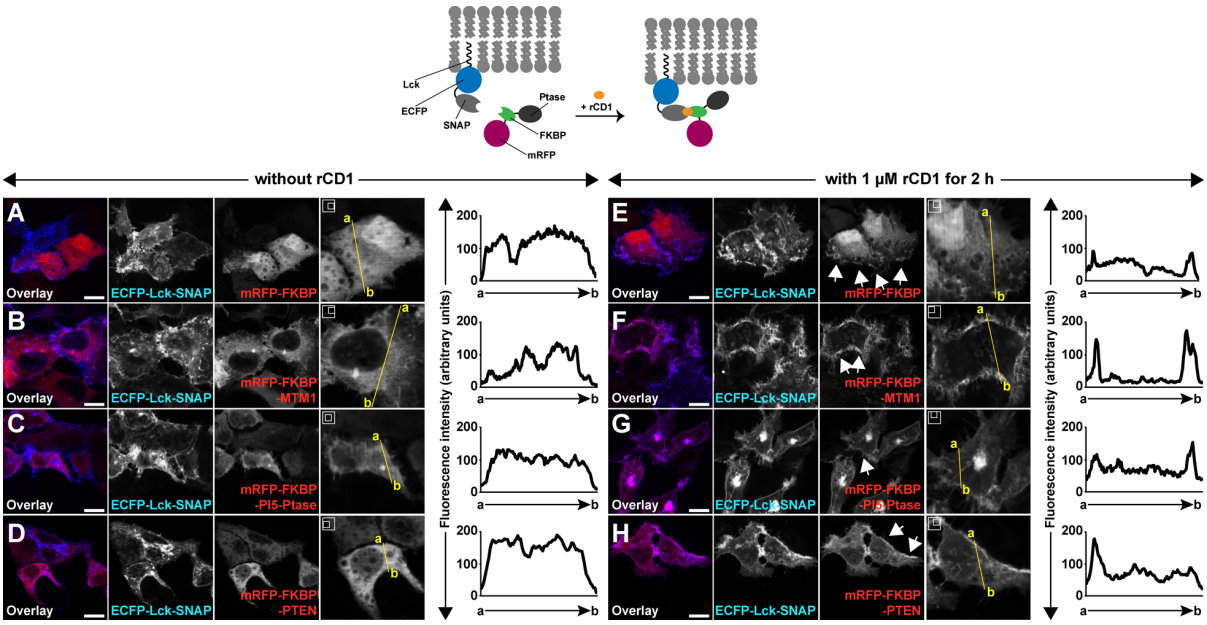

Fig. S5. rCD1-based recruitment of FKBP-constructs to the plasma membrane. Top: Schematic representation of the rCD1-based dimerization system for fast and efficient recruitment of proteins to the plasma membane. (A-H) Representative images of Flp-In T-Rex-EGFP-gephyrin HEK 293 cells cotransfected in their uninduced state (see *Materials and Methods*) with the plasma membrane anchor ECFP-Lck-SNAP (blue) and the different mRFP-FKBP constructs (red), as indicated. At 16 h post-transfection, the medium was replaced for 2h by serum-free DMEM (41966-029; Gibco) in the absence of rCD1 (A-D) or in the presence of 1 µM rCD1 (E-H). Note the cytosolic distribution of the mRFP-FKBP constructs in the absence of rCD1 (red channels in A-D). In contrast, a 2 h-treatment with 1 µM rCD1 efficiently induced translocation of the different mRFP-FKBP constructs to the plasma membrane (as indicated by arrows in E-H). Scale bars: 10 µm. Right panels in A-H: Magnifications of the corresponding channels of the mRFP-FKBP constructs as indicated in the rectangles shown in the upper left corners. Line-plots: Fluorescence intensity scans over the yellow lines of the corresponding images to their left, illustrating cytosolic distribution of the mRFP-FKBP constructs in the absence of rCD1 (A-D) and plasma membrane recruitment due to their interaction with ECFP-Lck-SNAP in the presence of 1 µM rCD1 (E-H).

FIGURE S6

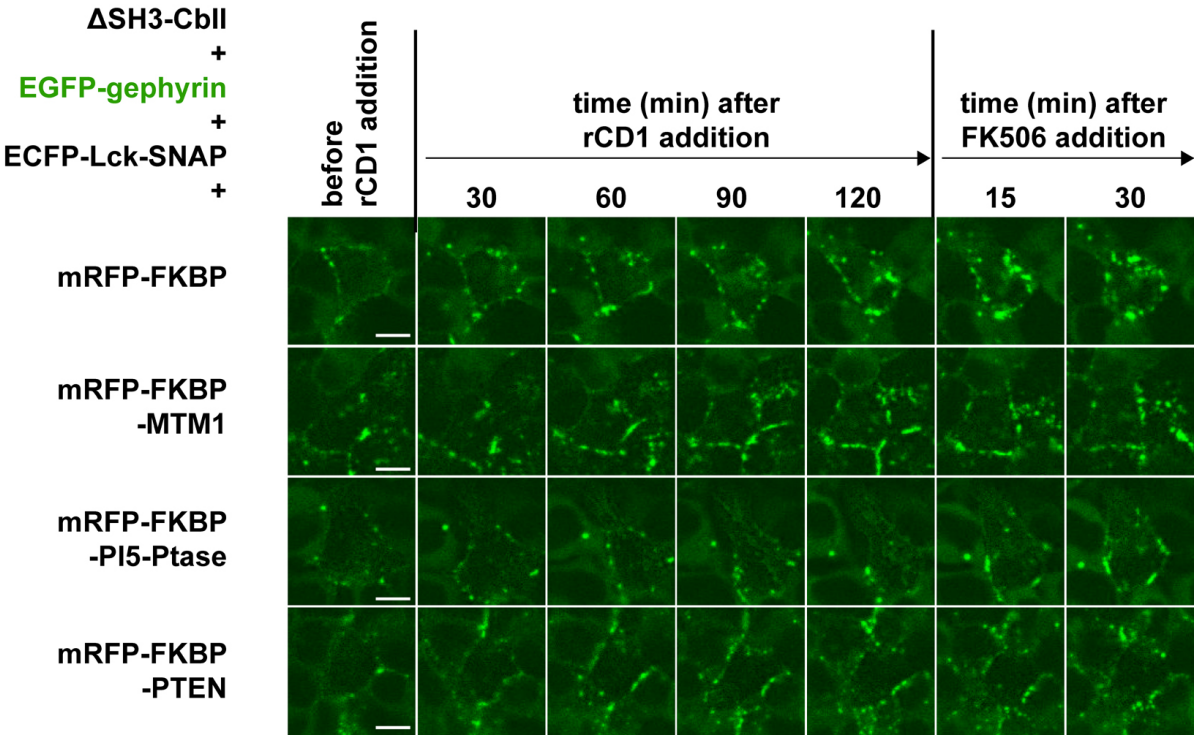

Fig. S6. Corresponding EGFP-gephyrin channels of the time-lapse confocal fluorescence images of Flp-In T-Rex-EGFP-gephyrin shown in Fig. 6. Cells were transfected and treated as indicated in the main text of the manuscript and in the legend to Fig. 6.

FIGURE S7

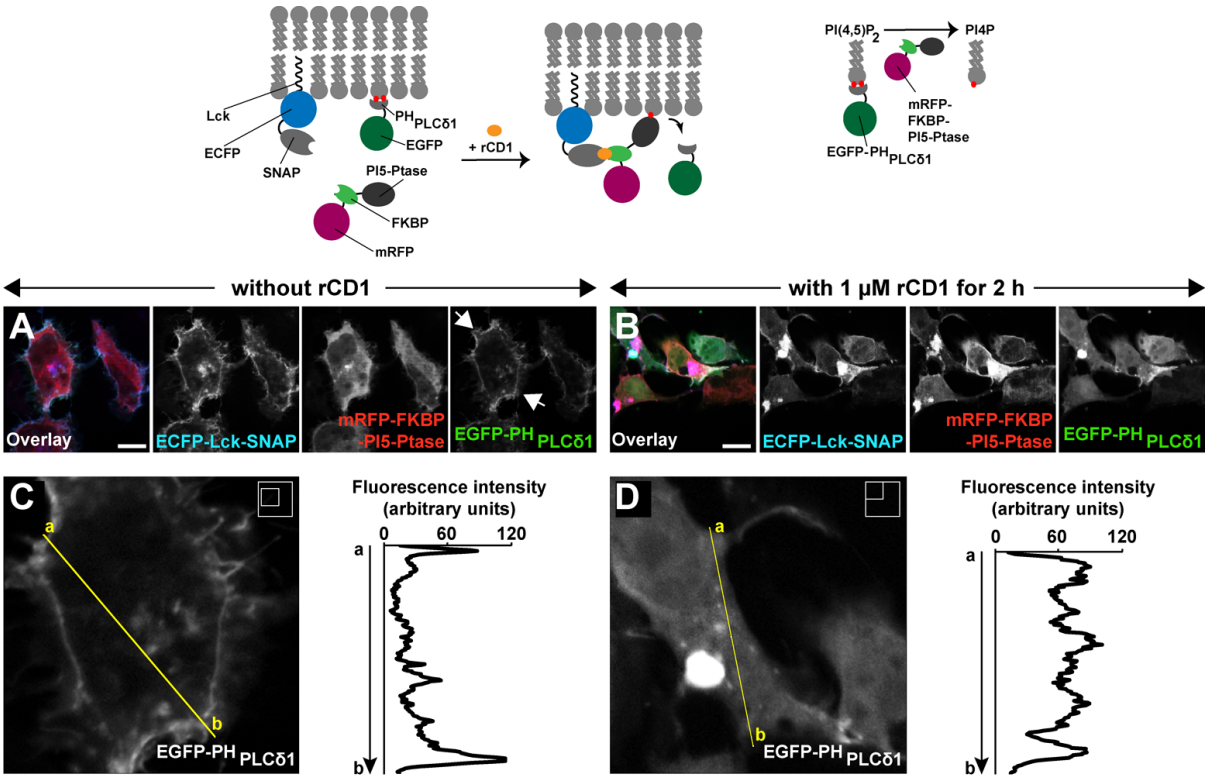

Fig. S7. rDC1-dependent plasma membrane recruitment of mRFP-FKBP-PI5-Ptase efficiently depletes PI(4,5)P_2. Top: Schematic representation of the rCD1-based recruitment of mRFP-FKBP-PI5-Ptase to the plasma membrane and the subsequent redistribution of EGFP-$PH_{PLC\delta1}$, a PI(4,5)P_2-specific probe. The rCD1-based dimerization of the membrane anchor ECFP-Lck-SNAP with mRFP-FKBP-PI5-Ptase leads to the conversion of PI(4,5)P_2 to PI4P. Thus, the EGFP-$PH_{PLC\delta1}$ probe cannot be anchored to the plasma membrane any more and redistributes into the cytosol. (A, B) Representative images of Flp-In T-Rex-EGFP-gephyrin HEK 293 cells cotransfected in their uninduced state (see *Materials and Methods*) with the plasma membrane anchor ECFP-Lck-SNAP (blue), mRFP-FKBP-PI5-Ptase (red) and EGFP-$PH_{PLC\delta1}$ (green), as indicated. At 16 h post-transfection, the medium was replaced for 2h by serum-free DMEM (41966-029; Gibco) in the absence of rCD1 (A) or in the presence of 1 µM rCD1 (B). Note the cytosolic distribution of mRFP-FKBP-PI5-Ptase (red) in the absence of rCD1 (A). In contrast, EGFP-$PH_{PLC\delta1}$ is mostly localized at the plasma mebrane (indicated by arrows) due to the accumulation of PI(4,5)P_2 at that compartment. (B) A 2 h-treatment with 1 µM rCD1 efficiently induced translocation of mRFP-FKB-PI5-Ptase to the plasma membrane and the subsequent redistribution of

EGFP-$PH_{PLC\delta1}$ into the cytosol, due to the depletion of $PI(4,5)P_2$. (C, D) Magnifications of the corresponding channels of EGFP-$PH_{PLC\delta1}$ in A and B, as indicated in the rectangles shown in the upper right corners. Line-plots: Fluorescence intensity scans over the yellow lines of the corresponding images to their left, illustrating plasma membrane localization of EGFP-$PH_{PLC\delta1}$ in the absence of rCD1 (C) and its cytosolic redistribution in the presence of 1 μM rCD1 (D).